HHS Public Access

Author manuscript

Neurobiol Dis. Author manuscript; available in PMC 2019 March 13.

Published in final edited form as:

Neurobiol Dis. 2018 October ; 118: 76–93. doi:10.1016/j.nbd.2018.07.004.

Reduced axonal surface expression and phosphoinositide sensitivity in K_v7 channels disrupts their function to inhibit neuronal excitability in *Kcnq2* epileptic encephalopathy.

Eung Chang Kim[1], **Jiaren Zhang**[1], **Weilun Pang**[1,*], **Shuwei Wang**[1,*], **Kwan Young Lee**[1], **John P. Cavaretta**[1], **Jennifer Walters**[1], **Erik Procko**[2,3], **Nien-Pei Tsai**[1,3], and **Hee Jung Chung**[1,3]

[1]Department of Molecular and Integrative Physiology, University of Illinois at Urbana-Champaign, Urbana, Illinois 61801, USA.

[2]Department of Biochemistry, University of Illinois at Urbana-Champaign, Urbana, Illinois 61801, USA.

[3]Neuroscience Program, and University of Illinois at Urbana-Champaign, Urbana, Illinois 61801, USA.

Abstract

Neuronal K_v7/KCNQ channels are voltage-gated potassium channels composed of $K_v7.2$/KCNQ2 and $K_v7.3$/KCNQ3 subunits. Enriched at the axonal membrane, they potently suppress neuronal excitability. *De novo* and inherited dominant mutations in $K_v7.2$ cause early onset epileptic encephalopathy characterized by drug resistant seizures and profound psychomotor delay. However, their precise pathogenic mechanisms remain elusive. Here, we investigated selected epileptic encephalopathy causing mutations in calmodulin (CaM)-binding helices A and B of $K_v7.2$. We discovered that R333W, K526N, and R532W mutations located peripheral to CaM contact sites decreased axonal surface expression of heteromeric channels although only R333W mutation reduced CaM binding to $K_v7.2$. These mutations also altered gating modulation by phosphatidylinositol 4,5-bisphosphate (PIP_2), revealing novel PIP_2 binding residues. While these mutations disrupted K_v7 function to suppress excitability, hyperexcitability was observed in neurons expressing $K_v7.2$-R532W that displayed severe impairment in voltage-dependent activation. The M518V mutation at the CaM contact site in helix B caused most defects in K_v7 channels by severely reducing their CaM binding, K^+ currents, and axonal surface expression. Interestingly, the M518V mutation induced ubiquitination and accelerated proteasome-dependent degradation of $K_v7.2$, whereas the presence of $K_v7.3$ blocked this degradation. Furthermore, expression of $K_v7.2$-M518V increased neuronal death. Together, our results demonstrate that epileptic encephalopathy mutations in helices A and B of $K_v7.2$ cause abnormal K_v7 expression and function by disrupting $K_v7.2$ binding to CaM and/or modulation by PIP_2. We propose that such multiple K_v7 channel defects could exert more severe impacts on neuronal excitability and health, and thus serve as pathogenic mechanisms underlying *Kcnq2* epileptic encephalopathy.

CORRESPONDING AUTHOR: Hee Jung Chung, Department of Molecular and Integrative Physiology, University of Illinois at Urbana-Champaign, 407 South Goodwin Avenue, 524 Burrill Hall, Urbana, IL 61801, USA.Telephone number: (217) 244-6839, chunghj@life.illinois.edu; chunghj@illinois.edu.

*These authors contributed equally.

DECLARATIONS OF INTERESTS: None

Keywords

K_v7 channels; *Kcnq2*; epileptic encephalopathy; mutation; calmodulin; phosphoinositide; excitability; surface expression; current

INTRODUCTION

Epilepsy is a common neurological disorder that strikes about 1.2% of the US population (www.cdc.gov). It is caused by excessive neuronal excitability characterized by seizures, which are abnormal and uncontrolled discharges of action potentials (Fisher et al., 2005). About 40% of all epilepsies are estimated to be caused by genetic factors including mutations in ion channels and occurs as early as infancy (Guerrini and Noebels, 2014). Among ion channels, neuronal K_v7/KCNQ potassium (K^+) channels have emerged as critical players in epilepsy because their agonist (ezogabine/retigabine) suppresses seizures in animal models and was clinically used as an anti-epileptic drug until 2017 (Blackburn-Munro et al., 2005; Gunthorpe et al., 2012; Large et al., 2012). Importantly, inherited and *de novo* mutations in *Kcnq2* and *Kcnq3* genes encoding $K_v7.2$ and $K_v7.3$ subunits are associated with early-onset epileptic disorders including benign familial neonatal epilepsy (BFNE) and epileptic encephalopathy (RIKEE database: www.rikee.org).

Neuronal K_v7 channels are mostly heterotetramers composed of $K_v7.2$ and $K_v7.3$ subunits (Shah et al., 2002; Wang et al., 1998), each subunit containing six transmembrane segments (S1–S6), cytoplasmic N- and C-termini, and the pore domain between the S5–S6 segments (Jentsch, 2000). Distributed throughout the brain including the hippocampus and neocortex (Cooper et al., 2001; Geiger et al., 2006; Pan et al., 2006; Weber et al., 2006) and in the peripheral nervous system (Dedek et al., 2001; Schwarz et al., 2006), K_v7 channels generate slowly activating and non-inactivating voltage-dependent K^+ current (Jentsch, 2000) that potently suppresses burst and repetitive firing of action potentials (APs) and contribute to resting membrane potential (Shah et al., 2008; Shah et al., 2002; Yue and Yaari, 2004; Yue and Yaari, 2006) (Tzingounis and Nicoll, 2008). Their current is also called ‘M-current’ since their inhibition by muscarinic agonists leads to a profound increase in AP firing (Brown and Passmore, 2009; Shah et al., 2002; Wang et al., 1998). Subcellularly, K_v7 channels are preferentially enriched at axonal plasma membrane compared to somatodendritic plasma membrane with highest concentration at the axonal initial segments (AIS) (Cavaretta et al., 2014; Chung et al., 2006), the critical sites for AP initiation and modulation (Clark et al., 2009). Their AIS localization is mediated by their interaction with ankyrin-G (Chung et al., 2006; Pan et al., 2006; Rasmussen et al., 2007), an essential component of the AIS (Bennett and Lorenzo, 2016; Jenkins et al., 2015). Consistent with their axonal enrichment, K_v7 channels regulate spike threshold, frequency, and shape (Gu et al., 2005; Peters et al., 2005; Shah et al., 2008; Soh et al., 2014; Tzingounis and Nicoll, 2008; Yue and Yaari, 2004; Yue and Yaari, 2006).

The first BFNE mutations were mapped to *Kcnq2* in 1998 (Biervert et al., 1998; Charlier et al., 1998; Singh et al., 1998). Since then, over 130 mutations in *Kcnq2* and *Kcnq3* have been associated with dominantly inherited BFNE in humans (RIKEE database: www.rikee.org).

Although BFNE is a rare disorder with transient appearance of seizures in neonates, the risk of recurring seizures later in life is 10–13% (Psenka and Holden, 1996). Furthermore, some BFNE mutations also accompany peripheral nerve hyperexcitability, myokymia, drug-refractory seizures, and developmental delay (Borgatti et al., 2004; Dedek et al., 2003; Dedek et al., 2001; Schmitt et al., 2005; Wuttke et al., 2007). Recently, multiple *de novo* mutations in $K_v7.2$ have been discovered in patients with early onset epileptic encephalopathy characterized by drug resistant seizures, psychomotor delay, developmental delay, distinct electroencephalogram (EEG) and neuroradiological abnormalities including white matter reduction and enlarged ventricles (Abidi et al., 2015; Kato et al., 2013; Kwong et al., 2015; Milh et al., 2013; Millichap et al., 2016; Numis et al., 2014; Saitsu et al., 2012; Weckhuysen et al., 2013; Weckhuysen et al., 2012; Zhang et al., 2016). Some *de novo* mutations of $K_v7.2$ are associated with Ohtahara and West syndromes, which are severe symptomatic drug resistant epilepsy with poor prognosis and profound psychomotor delay (Kato et al., 2013; Samanta et al., 2015). BFNE mutations have been extensively studied for their effects on K_v7 current and surface expression (Borgatti et al., 2004; Cavaretta et al., 2014; Chung et al., 2006; Dedek et al., 2003; Dedek et al., 2001; Maljevic and Lerche, 2014; Schmitt et al., 2005; Wuttke et al., 2007). However, pathogenic mechanisms underlying epileptic encephalopathy mutations of $K_v7.2$ have not been fully characterized. It is also unclear how BFNE and epileptic encephalopathy mutations of *Kcnq2* and *Kcnq3* ultimately lead to epilepsy with distinct severity.

Interestingly, one third of epileptic encephalopathy mutations in $K_v7.2$ are located in helices A-C within the large cytoplasmic C-terminal tail (Abidi et al., 2015; Kato et al., 2013; Kwong et al., 2015; Milh et al., 2013; Millichap et al., 2016; Numis et al., 2014; Saitsu et al., 2012; Weckhuysen et al., 2013; Weckhuysen et al., 2012; Zhang et al., 2016) that mediates channel assembly and interaction with multiple signaling molecules and proteins (Haitin and Attali, 2008) including phosphatidylinositol 4,5-bisphosphate (PIP_2) (Delmas and Brown, 2005; Suh and Hille, 2007; Suh et al., 2006), calmodulin (CaM) (Wen and Levitan, 2002; Yus-Najera et al., 2002), syntaxin-1A (Regev et al., 2009), and A-kinase-anchoring proteins (AKAPs) (Hoshi et al., 2005; Hoshi et al., 2003). PIP_2 binding is critical for proper function of neuronal K_v7 channels (Hernandez et al., 2008; Suh and Hille, 2002), although the precise PIP_2 binding residues in $K_v7.2$ are unknown. While helix C is responsible for subunit tetramerization (Schwake et al., 2006), CaM binds to helices A and B of all K_v7 subunits (Sachyani et al., 2014; Strulovich et al., 2016; Sun and MacKinnon, 2017; Xu et al., 2013; Yus-Najera et al., 2002). In crystal structure, CaM binds to the antiparallel coiled-coil architecture of helices A and B of $K_v7.2$ and $K_v7.4$ with helix A binding to CaM C-lobe, and helix B interacting with the CaM N-lobe (Strulovich et al., 2016; Xu et al., 2013; Yus-Najera et al., 2002). We have recently shown that disruption of CaM binding to $K_v7.2$ helix A impairs enrichment of heteromeric $K_v7.2$/ $K_v7.3$ channels at the axonal surface by promoting their retention in the endoplasmic reticulum (ER) (Cavaretta et al., 2014). Furthermore, decreasing CaM levels or dissociating CaM from $K_v7.2$ can reduce M-current density and enhance excitability in hippocampal neurons (Shahidullah et al., 2005). However, whether epileptic encephalopathy mutations in helices A-C alter CaM and PIP_2 affinity and subsequently disrupt K_v7 surface expression and function remains unknown.

In this study, we explored molecular pathogenetic effects of selected epileptic encephalopathy mutations (R333W, M518V, K526N, and R532W) in helices A and B of $K_v7.2$. We chose these specific mutations for several reasons. First, these mutations cause early-onset epileptic encephalopathy with drug-refractory seizures, profound psychomotor delay, and other behavioral comorbidities including autism and speech impairment. Second, we want to compare the effects of mutations buried within CaM contact sites (M518V in helix B) to those located at the periphery (R333W in helix A, K526N in helix B, and R532W in helix B-C linker). We found that the R333W, K526N, and R532W mutations located peripheral to CaM contact sites in helices A and B reduced axonal surface enrichment of heteromeric channels by 30% and disrupted their ability to suppress excitability in hippocampal neurons, although not all of them significantly impaired CaM binding or voltage-dependent activation. However, gating regulation by PIP_2 was impaired by R333W and R532W mutations, revealing these positively charged basic residues as novel PIP_2 modulation sites close to CaM contact sites. In contrast, M518V at the CaM contact site in helix B caused severe impairment in CaM binding, axonal surface expression, and voltage-dependent activation. Interestingly, this mutation also induced *de novo* ubiquitination and accelerated proteasome-dependent degradation of $K_v7.2$, whereas the presence of $K_v7.3$ blocked such degradation. Lastly, expression of $K_v7.2$-M518V enhanced neuronal injury and death. Taken together, these findings led to a surprising conclusion that pathogenic mechanisms of epileptic encephalopathy mutations in helices A-B of $K_v7.2$ involves a combination of distinct defects in K_v7 channels as well as neuronal injury depending on the nature of a mutation to disrupt CaM and PIP_2 affinity.

MATERIALS AND METHODS

Materials.

Antibodies used include anti-MAP2 (Millipore, AB5622), anti-ankyrin G (Neuromab, 75–146), anti-phospho IκBα Ser32 (14D4) (Cell Signaling, 2859), anti-GFP (Abcam, ab13970; Cell Signaling 2955S), anti-KCNQ2 (Alomone, APC-050; Neuromab, N26A/23), anti-KCNQ3 (Alomone, APC-051) anti-HA (Covance, MMS-101P, Cell Signaling, 3724 & 2369), anti-CaM (Cell Signaling, 4830), anti-GAPDH (Cell Signaling, 2118), HRP-conjugated secondary antibodies (The Jackson Laboratory, 715-005-151, 715-035-150, 711-035-152, 703-035-155) and Alexa Fluor dye-conjugated secondary antibodies (Invitrogen/Molecular Probes, A21202, A11072, A21076). Reagents used include 6-cyano-7-nitroquinoxaline-2,3-dione (CNQX), DL-2-amino-5-phosphonopentanoic (DL-AP5) and bicuculline (Sigma, C239, A5282, and 14343).

DNA Constructs and Mutagenesis.

Plasmids pcDNA3 with *Kcnq2* cDNA (Y15065.1) encoding $K_v7.2$ (CAA 75348.1), HA-$K_v7.2$, $K_v7.2$-A343D, *Kcnq3* cDNA (NM_004519) encoding $K_v7.3$, and HA-$K_v7.3$ have been described (Cavaretta et al., 2014; Chung et al., 2006; Schwake et al., 2000). *Kcnq2* mRNA (Y15065.1) is the first *Kcnq2* isoform isolated by positional cloning from fetal brain cDNA library (Biervert et al., 1998), and is identical to the reference sequence of *Kcnq2* transcript variant 3 (NM_004518.5) that contains a distinct 3’ UTR and lacks two alternate in-frame exons compared to the longest transcript variant 1 (NM_172107.3). In addition to

functional characterization of this transcript variant 3 (Biervert et al., 1998), we have previously reported that K_v7 channels composed of this shorter $K_v7.2$ isoform (CAA 75348.1) and $K_v7.3$ are preferentially localized to the axonal plasma membrane whereas BFNE mutations block this targeting in cultured hippocampal neurons (Cavaretta et al., 2014; Chung et al., 2006). Plasmid pJPA7 containing wild-type rat CaM was a gift from Dr. John Adelman (Oregon Health and Science University, Portland, OR) (Xia et al., 1998). The rat and human protein sequences of CaM are identical. EYFP-hCaM was a gift from Dr. Emanuel Strehler (Addgene plasmid # 47603). Epileptic encephalopathy mutations (R333W, M518V, R532W, K526N) were generated using the Quik Change II XL Site-Directed Mutagenesis Kit (Agilent) and verified by sequencing the entire cDNA construct.

Structural modeling and visualization.

The functional domains of $K_v7.2$ (NP_742105.1) from the longest transcript variant 1 (NM_172107.3) (Fig. 1A) were annotated based on multiple sources (Brown and Passmore, 2009; Chung, 2014; Strulovich et al., 2016; Xu et al., 2013) (RIKEE database: www.rikee.org). To model the interaction between calmodulin and $K_v7.2$ helices A and B, the sequence of human $K_v7.2$ helix A (amino acid E322-V367) was threaded to the crystal structure of Ca^{2+}-CaM bound to a chimeric Q3A-Q2B peptide (PDB 5J03) (Strulovich et al., 2016). The structure was relaxed with Rosetta (Leaver-Fay et al., 2011) using two rounds of sequential rotamer, side chain and backbone minimization, followed by rigid body minimization. The lowest scoring decoy from 20 runs was chosen as the final model. Site-specific mutations were made to the model in Rosetta followed by sequential rotamer, side chain, backbone, and rigid body minimization, and the lowest scoring of 20 decoys is presented in Figure 1D. Structures were visualized using the PyMOL Molecular Graphics System, Version 2.0 (Schrödinger, LLC). Amino acid residues R333, A343, M546, K554 and R560 in $K_v7.2$ isoform a (NP_742105.1) correspond to R333, A343, M518, K526 and R532 in $K_v7.2$ isoform c (CAA_75348.1).

Immunoprecipitation.

HEK293T cells cultured in 60 mm cell culture dish were transfected with plasmids (total 1.6 μg) containing $K_v7.2$ or EYFP-hCaM (1:1 ratio), or $K_v7.2$ and HA-$K_v7.3$ (1:1 ratio) using FuGENE6 transfection reagent (Promega). At 24 h post transfection, the entire cells were lysed and subjected to immunoprecipitation as described (Cavaretta et al., 2014) with small amount of rabbit anti-$K_v7.2$ antibody (5 μg) that could immunoprecipitate a fraction but not all of transfected $K_v7.2$ proteins. This allowed us to immunoprecipitate the equal amount of $K_v7.2$ proteins and analyze the effects of mutations on the amount of co-immunoprecipitated EYFP-hCaM and HA-$K_v7.3$ by immunoblotting with anti-GFP and anti-HA antibodies. To analyze $K_v7.2$ ubiquitination, immunoblotting with anti-HA antibody was performed on immunoprecipitated $K_v7.2$ proteins from cells transfected with plasmids containing HA-ubiquitin (0.3 μg), $K_v7.2$ (0.8 μg), with or without $K_v7.3$ (0.8 μg). For immunoblotting in Fig. S1, HEK293T cells were transfected with plasmids (total 1.6 μg) containing $K_v7.2$ wild-type or mutants with or without CaM. The lysates were analyzed by immunoblotting with anti-CaM, anti-$K_v7.2$, and anti-GAPDH antibodies.

Experimental animals and neuronal culture.

All procedures involving animals were reviewed and approved by the Institutional Animal Care and Use Committee at the University of Illinois Urbana-Champaign in accordance with the guidelines of the U.S National Institutes of Health (Protocols 15222). Primary dissociated hippocampal cultures were prepared from 18-day old embryonic rats and transfected with plasmids (total 1.0 μg) at 5 DIV as described (Cavaretta et al., 2014).

Immunocytochemistry.

Primary dissociated hippocampal cultures were prepared from 18-day old embryonic rats, transfected with plasmids (total 1.0 μg) at 5 DIV, and immunostaining for surface and total HA-K_v7.3/ K_v7.2 channels were performed at 48 h post transfection as previously described (Cavaretta et al., 2014). Immunostaining for surface and total K_v7 subunits and AIS markers (ankyrin-G and phospho IκBα-Ser32) in hippocampal neurons and HEK293T cells were performed at 24–48 h post transfection as described (Cavaretta et al., 2014). Fluorescence images were acquired as described (Cavaretta et al., 2014) using Zeiss Axiovert 200M inverted microscope equipped with AxioCam HRm Camera and Axiovert software, and stored with no further modification as ZVI and 16-bit TIFF files. Within one experiment, the images were acquired using the same exposure time to compare the fluorescence intensity of the neurons transfected with different constructs. The analyses of surface and total HA-K_v7.3/ K_v7.2 channels in Figure 3 were performed only from the healthy transfected neurons identified by differential interference contrast (DIC) imaging and the fluorescence imaging of HA-K_v7.3 immunostaining. If the transfected neurons had beaded or broken dendrites or axons, or damaged soma (i.e. dead neurons), then they were excluded from analyses. The background-subtracted mean fluorescence intensity of the soma, the axon within 0–30 μm of the beginning of the axon (AIS), the axon between 50–80 μm from the beginning of the axon (distal axon), and the major primary dendrites were quantified using ImageJ Software (National Institutes of Health) as described (Cavaretta et al., 2014). In Figure 8, the number of all K_v7.2-transfected neurons, the number of K_v7.2-transfected dead neurons, and the number of the K_v7.2-transfected neurons showing prominent immunostaining of endogenous ankyrin-G at the AIS were counted.

Electrophysiology.

Whole cell patch clamp recordings were made at room temperature (20°C–22°C) using a Multiclamp 700B amplifier, acquired with a Digidata 1440A interface, and analyzed with pClamp 10.6 and Clampfit 10.6 (Molecular Devices). Current-clamp recordings were performed from cultured hippocampal neurons, filtered at 2 kHz, and digitized at 10 kHz as previously described (Cavaretta et al., 2014). At 24–48 hr post transfection with plasmids (total 1 μg) including pEGFPN1 and pcDNA3-K_v7.2, spike trains were evoked from untransfected or GFP-positive neurons as described (Cavaretta et al., 2014) by delivering constant somatic current pulses of 500 ms in the range 0 to 200 pA at a holding potential of −60 mV and in the presence of the fast synaptic transmission blockers CNQX (20 μM), DL-AP5 (100 μM) and bicuculline (20 μM).

Voltage clamp recording of K^+ currents were carried out in Chinese hamster ovary (CHO hm1) cells (kind gifts from Dr. Naoto Hoshi, University of California, Irvine), filtered at 1

kHz, and digitized at 10 kHz as described (Kosenko et al., 2012; Miceli et al., 2015). Cells were plated on 12mm glass coverslips (Warner Instrument, 10^5 cells per coverslip) coated with Poly D-lysine (0.1 mg/ml) and transfected at 24 h post plating with plasmids (total 1 μg) including pEGFPN1 (0.2 μg) and pcDNA3-K_v7.2 WT or mutant (0.8 μg). At 24–48 h post transfection, recordings from GFP-positive cells were performed in external solution containing (in mM): 138 NaCl, 5.4 KCl, 2 $CaCl_2$, 1 $MgCl_2$, 10 D-glucose, and 10 HEPES (pH 7.4, 307–312 mOsm). Recording pipettes had a resistance of 3–5 MΩ filled with internal solution containing (in mM): 140 KCl, 2 $MgCl_2$, 10 EGTA, 10 HEPES, 5 Mg-ATP, (pH 7.4 with KOH, 290–300mOsm). Resting membrane potential was determined in current clamp after achieving the whole-cell configuration. To record K^+ current, cells were held at −80 mV and then voltage steps were applied for 1.5 s from −100 mV to 20 mV in 10 mV increments, followed by an isopotential pulse at 0 mV of 300 ms duration. To examine PIP_2 sensitivity of K_v7.2 channels, the recording was repeated with internal solution containing diC8-PIP_2 (100 μM).

All currents were measured under whole-cell voltage clamp with pipette and membrane capacitance cancellation. Leak subtracted currents were computed by subtracting leak currents from peak current at all voltage steps. Leak currents were defined as non-voltage-dependent current from GFP-transfected cells. Current densities (expressed in picoamperes per picofarad) were calculated as leak-subtracted peak K^+ currents divided by capacitance (C). For Figures 4B and 5B, the leak-subtracted peak current density at each voltage step was measured and plotted as a function of the preceding voltages. For Figures 5C and 5E, the normalized conductance (G / Gmax) was plotted as a function of voltage steps. No corrections were made for liquid junction potentials. To measure the channel kinetics, current traces were fitted with a double exponential function of the following form: $y = A_f\exp(\tau/\tau_f) + A_s\exp(\tau/\tau_s)$, where A_f and A_s indicate the fractions of the fast and slow exponential components of the current, respectively, and τ_f and τ_s indicate the time constants of these components. The time constant representing the weighted average of the fast and slow components of current activation was calculated with the following equation; $\tau = (\tau_f A_f + \tau_s A_s)/(A_f+A_s)$. For Table 2, the leak-subtracted currents were then fit to a Boltzmann distribution of the following form: $y = y_{max} / [1/\exp(V_{1/2}-V)/k]$, where V is the test potential, $V_{1/2}$ the half-activation potential, and k the slope factor.

Statistical Analyses.

All analyses are reported as mean ± SEM. Using Origin 9.1 (Origin Lab), the Student *t* test and one-way ANOVA with post-ANOVA Tukey's and Fisher's multiple comparison tests were performed to identify the statistically significant difference with a priori value (p) < 0.05 between 2 groups and for >3 groups, respectively.

RESULTS

K_v7.2 binding to CaM is severely decreased by M518V mutation in CaM contact site and modestly reduced by R333W mutation located peripheral to CaM contact site.

To date, 50 missense mutations in K_v7.2 have been associated with early-onset epileptic encephalopathy. Mapping 21 epileptic encephalopathy mutations to the cytoplasmic C-

terminal tail of $K_v7.2$ revealed their location at 4 distinct domains: helix A that contains consensus IQ motif for CaM binding and interacts with CaM C-lobe (Gamper and Shapiro, 2003; Strulovich et al., 2016; Yus-Najera et al., 2002), helix B that binds to CaM N-lobe and has preferential affinity to Ca^{2+}-bound CaM *in vitro* (Alaimo et al., 2012; Strulovich et al., 2016; Xu et al., 2013), the linker from helix B to helix C, and helix C that mediates subunit interaction (Schwake et al., 2006)(Fig. 1A). Epileptic encephalopathy mutations are clustered in helix A and helix B, but no mutations are found in the linker between helix A and helix B. This interesting trend of mutation clustering at or near CaM binding sites suggests that a molecular pathogenetic mechanism of epileptic encephalopathy involves disruption of $K_v7.2$ binding to CaM.

To test if epileptic encephalopathy mutations in helices A and B and the helix B-C linker impair $K_v7.2$ interaction with CaM, we introduced point mutations in helix A (R333W), helix B (M518V, K526N) and helix B-C linker (R532W) in $K_v7.2$ (protein accession CAA 75348.1) (Fig. 1A, B). We selected these epileptic encephalopathy mutations to compare the effects of mutations buried within CaM contact sites (M518V) to those located at the periphery (R333W, K526N, and R532W) (Fig. 1C, D). The A343D mutation located in the consensus IQ motif of helix A was included in this study as a control (Fig. 1B–D) because this nonpathogenic variant was previously shown to disrupt CaM interaction with $K_v7.2$ (Alaimo et al., 2009; Cavaretta et al., 2014; Wen and Levitan, 2002). Indeed, our modeling of $K_v7.2$ helices A-B structure with Ca^{2+}-bound CaM predicted that the A343D mutation at the CaM C-lobe contact site brings a desolvated acidic group into a buried hydrophobic interface (Fig. 1D). This creates steric clashes which result in rotamer shifts of surrounding side chains and subsequent destabilization of the interaction between $K_v7.2$ helix A with CaM C-lobe (Fig. 1D).

We then performed co-immunoprecipitation studies in the presence of the Ca^{2+} chelator EGTA from HEK293T cells transfected with $K_v7.2$ and CaM N-terminally tagged with yellow fluorescent protein (YFP) (Fig. 2A, B). We first noticed that the expression of $K_v7.2$-A343D and $K_v7.2$-M518V was consistently lower compared to wild type $K_v7.2$ proteins in the presence of YFP-CaM although equal amounts of each plasmid were transfected in HEK293T cells (Fig. 2A, B). To immunoprecipitate the same amount of wild-type and mutant $K_v7.2$ and compare the effect of mutations on $K_v7.2$ coimmunoprecipitation with CaM, we therefore used small amount of anti-$K_v7.2$ N-terminal antibodies that could immunoprecipitate a fraction but not all of transfected $K_v7.2$ subunits from the large amount of transfected cell lysate.

Although similar amounts of wild type and mutant $K_v7.2$ proteins were immunoprecipitated, YFP-CaM co-immunoprecipitated with wild type Kv7.2 but not Kv7.2 containing A343D mutation in the CaM contact site within helix A (Fig. 2A, B), consistent with our previous report (Cavaretta et al., 2014). The M518V mutation is located at the CaM N-lobe contact site within a completely buried hydrophobic region of helix B (Fig. 1C, D). This mutation is expected to create a large void at the interface center with little compensatory conformational changes of the neighboring residues, thereby destabilizing the helix B-CaM interface (Fig. 1D). Consistent with our prediction, M518V mutation severely decreased coimmunoprecipitation of apoCaM with $K_v7.2$ by 85% (Fig. 2A, B). CaM cotransfection

also increased the expression of wild-type $K_v7.2$ and $K_v7.2$-M518V but not $K_v7.2$-A343D (Fig. S1), supporting our coimmunoprecipitation findings that CaM binding to $K_v7.2$ is severely reduced but not abolished by M518V mutation.

The R333W mutation located proximal to the CaM C-lobe contact site of helix A introduces an indole ring which can pack against hydrophobic residues of CaM (V92, F93, and L113) to make alternative favorable contacts, and thus is expected to have mild impact on $K_v7.2$ helix A interaction with CaM C-lobe (Fig. 1D). Consistently, the R333W mutation reduced $K_v7.2$ expression and its interaction with apoCaM by 20% (Fig. 2A, B). The K526N mutation is distal to the CaM N-lobe contact interface in Kv7.2 (Fig. 1C). The K526N mutation is anticipated to modestly affect helix B binding to CaM N-lobe due to the loss of a solvent-exposed electrostatic contact to E48 of CaM (Fig. 1D). Although the K526N mutation decreased $K_v7.2$ coimmunoprecipitation with apoCaM by 35%, this change did not reach statistical significance (Fig. 2A, B). Consistent with the location of R532W beyond helix B (Fig. 1B, C), the R532W mutation had no effect on $K_v7.2$ binding to apoCaM (Fig. 2A, B).

To test if epileptic encephalopathy mutations in helices A and B and the helix B-C linker impair $K_v7.2$ interaction with $K_v7.3$, we repeated co-immunoprecipitation studies in HEK293T cells transfected with $K_v7.2$ and HA-$K_v7.3$ which is extracellularly tagged with a HA epitope (Fig. 2C, D). Although an increasing trend was observed in $K_v7.2$-M518V coimmunoprecipitation with HA-$K_v7.3$, none of the tested mutations significantly affected $K_v7.2$ binding to HA-$K_v7.3$ (Fig. 2C, D).

Enrichment of K_v7 channels at the axonal surface is severely decreased by M518V mutation, and modestly reduced by R333W, K526N, and R532W mutations.

We have previously shown that A343D mutation in the IQ motif of $K_v7.2$ helix A disrupts CaM binding to $K_v7.2$ and blocks preferential targeting of heteromeric K_v7 channels to the axonal membrane in hippocampal neurons by inhibiting their trafficking from the ER to the axons (Cavaretta et al., 2014) (Fig. 2A, B, Fig. S2). These previous findings together suggest that CaM binding to helix A of $K_v7.2$ is critical for K_v7 targeting to the axonal surface. Therefore, we next tested if epileptic encephalopathy mutations in helices A and B of $K_v7.2$ affect surface density of heteromeric K_v7 channels in hippocampal neurons.

We performed surface immunostaining of $K_v7.3$ containing an extracellular HA epitope (HA-$K_v7.3$) (Cavaretta et al., 2014) since antibodies that recognize extracellular domains of endogenous $K_v7.2$ and $K_v7.3$ are not available. HA-$K_v7.3$ has been shown to display K^+ current and surface expression in Xenopus oocytes coexpressing $K_v7.2$ (Schwake et al., 2006; Schwake et al., 2000). We have previously demonstrated in cultured hippocampal neurons that homomeric HA-$K_v7.3$ channels are not expressed on the plasma membrane, whereas co-transfection of $K_v7.2$ results in robust axonal surface expression of HA-$K_v7.3$ (Cavaretta et al., 2014; Chung et al., 2006). Consistent with our previous reports, strong immunostaining of HA-$K_v7.3$ was detected on the axonal plasma membrane compared to somatodendritic plasma membrane in cultured hippocampal neurons cotransfected with $K_v7.2$ (Fig. 3A–C), resulting in the surface “Axon / Dendrite” ratio of 3.5 ± 0.4 (Fig. 3D). The highest intensity of HA-$K_v7.3$/$K_v7.2$ channels was observed at the AIS (Fig. 3A–C).

In contrast, the M518V mutation, which severely reduced CaM binding to $K_v7.2$ (Fig. 2A, B), decreased surface expression of heteromeric HA-$K_v7.3$/$K_v7.2$ channels at the distal axons to the level of untransfected neurons (Fig. 3A–C), reducing the surface "Axon / Dendrite" ratio to 1.1 ± 0.1 (Fig. 3D). The surface and total expression of HA-$K_v7.3$/$K_v7.2$-M518V at the AIS and the soma was also reduced to a third and a half of wild type channels, respectively (Fig. 3A–C). No significant expression of these mutant channels was seen at the dendrites (Fig. 3C). The weak but detectable expression of heteromeric HA-$K_v7.3$/$K_v7.2$-M518V mutant channels at the AIS (Fig. 3A–D) is in sharp contrast to the complete absence of heteromeric A343D mutant channels from the AIS and axons (Fig. S2)(Cavaretta et al., 2014).

The R333W and K526N mutations decreased axonal surface expression of heteromeric HA-$K_v7.3$/$K_v7.2$ channels (Fig. 3A–C) and the surface "Axon / Dendrite" ratio by 30% (Fig. 3D), consistent with decreasing trend in CaM binding to $K_v7.2$-R333W and $K_v7.2$-K526N (Fig. 2A, B). Reduction in total expression was also seen in the soma for heteromeric HA-$K_v7.3$/$K_v7.2$ channels harboring R333W and K526N mutation (Fig. 3C). Surprisingly, the R532W mutation also decreased overall surface expression of heteromeric HA-$K_v7.3$/$K_v7.2$ channels (Fig. 3A–C) and reduced the surface "Axon / Dendrite" ratio by 30% (Fig. 3D) although this mutation did not affect $K_v7.2$ binding to CaM (Fig. 2A, B). These data provide strong evidence that all tested epileptic encephalopathy mutations at or near CaM-binding domains reduced preferential enrichment of heteromeric K_v7 channels at the axonal surface.

Voltage-dependent activation of $K_v7.2$ channels is decreased by R532W mutation in helix B-C linker and abolished by M518V mutation in helix B.

Mutant $K_v7.2$ channels deficient in CaM binding have been previously reported to be non-functional (Wen and Levitan, 2002), whereas CaM cotransfection has shown to increase current density of $K_v7.2$ channels (Ambrosino et al., 2015; Soldovieri et al., 2016). To test if epileptic encephalopathy mutations in helices A and B of $K_v7.2$ affect voltage-dependent activation of $K_v7.2$ channels, we performed whole-cell patch clamp recording in CHO hm1 cells, a well-established system to measure K^+ current through exogenously expressed K_v7 channels (Kosenko et al., 2012). The patch pipette solution contained EGTA to sequester free Ca^{2+}. In CHO hm1 cells transfected with GFP, the resting membrane potential was −10.2 ± 0.7 mV (Table 1), consistent with very low expression of endogenous K^+ channels (Gamper et al., 2005). Application of depolarizing voltage steps from −100 to +20 mV in GFP-transfected cells generated very little inward and outward currents (Fig. S3), which displayed no obvious voltage-dependence and reversed around −25.6 ± 1.6 mV (Tables 1, 2).

In cells transfected with GFP and wild type $K_v7.2$, application of voltage steps produced slowly activating outward K^+ currents at a threshold voltage around −40 mV (Fig. 4A–E Fig. S3). Consistently, the resting membrane potential of these cells was hyperpolarized to −37.0 ± 1.1 mV (Table 1), indicating the significant presence of K^+ currents. In contrast, $K_v7.2$-A343D channels failed to display voltage-dependent outward K^+ current and did not alter resting membrane potentials (Fig. 4A–E, Supplemental Fig. 3, Tables 1, 2), consistent with their retention in the ER (Alaimo et al., 2009; Cavaretta et al., 2014; Etxeberria et al., 2008). The $K_v7.2$-M518V channels produced very small outward currents that lacked voltage-

dependence (Fig. 4A–D, Fig. S3) but were sufficient to hyperpolarize membrane potential to −28.5 ± 1.6 mV (Table 1). In sharp contrast to HEK293T cells (Fig. 2), the total protein expression of K_v7.2-A343D and K_v7.2-M518V was comparable to the wild-type K_v7.2 in CHO hm1 cells (Fig. 4E).

The cells expressing K_v7.2-R333W or K_v7.2-K526N generated slowly activating voltage-dependent outward K^+ currents that were slightly smaller or larger than the cells expressing wild type K_v7.2 (Fig. 4A–D, Fig. S3, Table 1–2), although this difference did not reach statistical significance. Consistent with this trend, decreased K_v7.2-R333W expression and increased K_v7.2-K526N expression was observed in CHO hm1 cells (Fig. 4E). K_v7.2-K526N channels also displayed a small left shift in voltage-dependence at −50 mV to −30 mV (Fig. 4D). Although total expression of K_v7.2-R532W was comparable to wild-type K_v7.2 (Fig. 4E), the cells expressing K_v7.2-R532W generated 40% less outward K^+ currents (Fig. 4A–C, Fig. S3) with a right shift in voltage-dependence at −10 mV to +10 mV (Fig. 4D). In addition, the R532W mutation significantly slowed the channel activation (Table 2). These findings indicate that the M518V and R532W mutations significantly impaired current expression of K_v7.2 channels.

PIP_2 stimulation of K_v7.2 current is decreased by R333W and R532W mutations and increased by K526N mutation.

Phosphatidylinositol-4,5-bisphosphate (PIP_2) is critical for proper function of all K_v7 channels (Gamper and Shapiro, 2007; Logothetis et al., 2015). Previous studies have suggested that PIP_2-dependent potentiation of K_v7 currents may be mediated by the regions close to helices A and B and regulated by Ca^{2+}-bound CaM (Hernandez et al., 2008; Tobelaim et al., 2017b). In K_v7.1, PIP_2 interacts with lysine residues in helix B, where Ca^{2+}-bound CaM competes to stabilize the channel open state (Tobelaim et al., 2017b). The analogous basic amino acid residues in helix B of K_v7.2 are structurally close to the beginning of helix A, which contains another cluster of positively charged residues K331, R332, and R333 (Fig. 1B), suggesting that EE mutations located peripheral to CaM contact site in helix B (R333W, K526N, R532W) may alter PIP_2 sensitivity of K_v7.2 channels. To test this possibility, we repeated whole-cell patch clamp recording in CHO hm1 cells in the presence of short-chained diC8-PIP_2 (100 μM) in the intracellular solution.

Addition of diC8-PIP_2 induced a 50% increase in voltage-activated outward K^+ currents through wild type K_v7.2 channels compared to those measured in the absence of diC8-PIP_2 (Fig. 5A–D, Fig. S4). Addition of diC8-PIP_2 also caused a left shift in voltage-dependence at −60 mV to −0 mV (Fig. 5C). In contrast, R333W mutation abolished the diC8-PIP_2-mediated increase in current density (Fig. 5A–D, Fig. S4). In the absence of diC8-PIP_2, K_v7.2-R532W channels displayed a >50% reduction in voltage-dependent outward K^+ currents compared to wild-type channels (Fig. 4B, 5D). No further increase in outward K^+ currents through K_v7.2-R532W channels was observed in the presence of diC8-PIP_2 (Fig. 5A–D). Introduction of diC8-PIP_2 produced larger K^+ currents through K_v7.2-K526N channels compared to those measured without diC8-PIP_2 (Fig. 5A–B), caused a left shift in voltage-dependence at −30 mV to 10 mV (Fig. 5C), and further hyperpolarized the resting membrane potential to −53.1 ± 2.2 mV from −43.1 ± 0.8 mV (Table 1). Surprisingly, the

currents through $K_v7.2$-K526N channels in the presence of diC8-PIP_2 were significantly larger than those through wild type channels (Fig. 5A–D, Fig. S4). These results together indicate that R333W and R532W mutations reduced whereas K526N mutation enhanced sensitivity of $K_v7.2$ channels to gating modulation by PIP_2.

Hippocampal neuronal excitability is reduced upon expression of wild type $K_v7.2$ but not $K_v7.2$ containing R333W, K526N, or R532W mutation.

Since axonal K_v7 channels inhibit excitability of hippocampal neurons (Shah et al., 2011; Shah et al., 2008), multiple defects in K_v7 axonal surface density and current expression induced by epileptic encephalopathy mutations (Fig. 2–5) could impair their function in suppressing neuronal excitability. To test this, we performed whole cell patch clamp recording of action potentials in cultured hippocampal neurons transfected with wild-type or mutant $K_v7.2$. Since rat hippocampal neurons in dissociated culture display mRNA and protein expression of $K_v7.2$ and $K_v7.3$ as well as K_v7 current (Lee and Chung, 2014; Lee et al., 2015)(Fig.S5–6), we hypothesized that transiently expressed wild-type $K_v7.2$ would form functional homomeric channels with endogenous $K_v7.2$ and heteromeric channels with endogenous $K_v7.3$ at the axonal plasma membrane and reduce excitability (Fig. 6A). Consistent with this hypothesis and our previous reports (Cavaretta et al., 2014), transfection of wild type $K_v7.2$ increased expression of $K_v7.2$ about 4-fold compared to untransfected neurons and decreased action potential firing rates compared to untransfected neurons and GFP-expressing neurons for all current injections from 40 pA (Fig. 6B–E, Fig. S6). Although transfection of wild type $K_v7.2$ did not affect passive intrinsic properties of hippocampal neurons (Table 3), $K_v7.2$ expression increased AP half-width and AP decay time compared to untransfected neurons and GFP-expressing neurons (Table 4) most likely due to increased K^+ efflux through transfected $K_v7.2$-containing channels. There was no change in AP height and AP rise time (Table 4), which are largely regulated by Na^+ influx through endogenous voltage-gated sodium channels.

In contrast, transfection of $K_v7.2$-R333W, $K_v7.2$-K526N, or $K_v7.2$-R532W did not reduce action potential firing frequency (Fig. 6B–D), although their expression at the AIS is comparable to wild-type $K_v7.2$ (Fig. 6E). Interestingly, action potential firing rates induced by 30–120 pA injections were significantly enhanced in neurons expressing $K_v7.2$-R532W compared to neurons expressing GFP alone (Fig. 6B–D), suggesting that hippocampal neurons expressing $K_v7.2$-R532W are hyperexcitable. Expression of mutant $K_v7.2$ did not affect membrane capacitance, input resistance, and resting membrane potential compared to untransfected or GFP-transfected neurons (Table 3). Furthermore, none of these mutations affected AP height, half width, and rise and decay times compared to untransfected or GFP-transfected neurons (Table 4). Together, these data indicate that $K_v7.2$ proteins containing R333W, K526N, and R532W mutations are defective in reducing excitability of hippocampal neurons.

$K_v7.2$-M518V proteins undergo ubiquitination and proteasome-dependent degradation whereas $K_v7.3$ coexpression prevents this degradation.

When investigating the effect of M518V mutation in hippocampal neuronal excitability, we faced difficulty in patching $K_v7.2$-M518V transfected hippocampal neurons due to frequent

plasma membrane rupture. We had similar difficulties with CHO hm1 cells expressing K_v7.2-M518V in Figure 4. These results suggest that M518V mutation may cause other dysfunction that could compromise neuronal health, in addition to severely reducing current and axonal surface expression of K_v7 channels (Fig. 3–4).

Indeed, we observed accelerated degradation of K_v7.2 proteins containing M518V or A343D mutation in HEK293T cells by 24 h post transfection (Fig. 7A, B), although both wild type and mutant K_v7.2 proteins were equally expressed at 10 h post transfection (Fig. 7A). Interestingly, only K_v7.2-M518V proteins were heavily ubiquitinated (Fig. 7C, D). Our immunostaining revealed that M518V mutation decreased K_v7.2 expression by half whereas treatment with the proteasome inhibitor MG132 blocked this degradation (Fig. 7E, F), suggesting that ubiquitinated K_v7.2-M518V proteins underwent proteasome-dependent degradation. MG132 treatment also induced aggregation of K_v7.2-M518V proteins (Fig. 7E), consistent with previous reports that inhibition of proteasome-dependent degradation drives polyubiquitinated proteins in the ER to form large aggregates (Jaeger and Wyss-Coray, 2009).

Surprisingly, cotransfection of K_v7.3 subunits blocked degradation (Fig. 2C, D) but not ubiquitination of K_v7.2-M518V proteins (Fig. S7A), resulting in a 2-fold increase in their expression compared to expression of K_v7.2-M518V alone (Fig. 8A–B, S7B). In the presence of K_v7.3, abnormal accumulation of K_v7.2-M518V proteins was also evident compared to wild-type K_v7.2 expression (Fig. S7B). These findings indicate that K_v7.3 prevents degradation of ubiquitinated K_v7.2-M518V proteins and stabilizes their expression.

Expression of K_v7.2-M518V induces cell and nuclei shrinkage and hippocampal neuronal injury.

Intracellular accumulation of misfolded proteins has been shown to induce ER stress and cause cell death (Su et al., 2011; Tyedmers et al., 2010). Indeed, we observed that expression of K_v7.2-M518V increased the number of transfected HEK293T cells that underwent cell shrinkage, a hallmark of the early events during programmed cell death by apoptosis (Bortner and Cidlowski, 2002; Maeno et al., 2000), compared to wild type K_v7.2 expression (Fig. 8A, C). Transfection of K_v7.2-M518V and K_v7.3 in HEK293T cells also caused cell shrinkage compared to coexpression of wild type K_v7.2 and K_v7.3 (Fig. 8A, C). Nuclei condensation, a late-stage event in apoptosis (Bortner and Cidlowski, 2002; Maeno et al., 2000), was observed in cells expressing K_v7.2-M518V alone compared to those expressing wild type Kv7.2 and was further enhanced by cotransfection of K_v7.3 (Fig. 8A, D). These results indicate that expression of K_v7.2-M518V induces cell death and K_v7.3 co-expression aggravates this effect in HEK293T cells.

To test if expression of K_v7.2-M518V may compromise neuronal health, we examined the morphology of hippocampal neurons transfected with wild type K_v7.2 or K_v7.2-M518V. At 48 h post transfection, fluorescence imaging of co-transfected GFP and differential interference contrast (DIC) imaging was employed to identify the dead neurons, which displayed damaged soma and beaded or broken neurites. Recent studies have shown that disruption of the AIS by rapid, irreversible proteolysis of cytoskeleton proteins including ankyrin-G and βIV spectrin occurs upon neuronal injury independently of cell death or axon

degeneration (Schafer et al., 2009). Therefore, we also examined the presence of ankyrin-G as an indication of health (Fig. 8E). Despite similar expression of wild type $K_v7.2$ and $K_v7.2$-M518V proteins in hippocampal neurons (Fig. 6E, S6), we observed a significant decrease in the number of GFP-positive neurons expressing $K_v7.2$-M518V that showed prominent ankyrin-G immunostaining at the AIS compared to neurons expressing GFP alone or together with wild type $K_v7.2$ (Fig. 8E, F). Concurrently, expression of GFP and $K_v7.2$-M518V increased the number of dead transfected neurons compared to expression of GFP with or without wild type $K_v7.2$ (Fig. 8F). In the presence of HA-$K_v7.3$, expression of $K_v7.2$-M518V also increased the number of dead transfected neurons and decreased the number of transfected neurons with ankyrin-G immunostaining compared to expression of wild type $K_v7.2$ (Fig. 8G). These results suggest that expression of $K_v7.2$-M518V increases neuronal injury and death.

DISCUSSION

In this study, we investigated the molecular pathogenetic effects of *de novo* epileptic encephalopathy mutations concentrated at and near helices A and B of $K_v7.2$ (Fig. 1). *In vitro* studies with $K_v7.2$ helix A or helix B have shown that apoCaM binds equally to helices A and B (Xu et al., 2013) whereas Ca^{2+}-bound CaM favors interaction with helix B (Alaimo et al., 2012; Gamper and Shapiro, 2003; Xu et al., 2013; Yus-Najera et al., 2002). We have previously shown that CaM binding to the IQ motif of $K_v7.2$ helix A is critical for the ER export and axonal surface expression of K_v7 channels (Cavaretta et al., 2014), which are responsible for potently suppressing spontaneous and bursting firing of APs in hippocampal neurons (Shah et al., 2011; Shah et al., 2008). Our characterization of selected epileptic encephalopathy mutations of K_v7 helix A (R333W), helix B (M518V, K526N) and helix B-C linker (R532W) revealed the unexpected findings that each mutation displayed a unique combination of K_v7 channel defects including disruption of CaM binding to $K_v7.2$ (Fig. 2), reduction in axonal surface expression of K_v7 channels (Fig. 3), changes to voltage-dependent activation and PIP_2 sensitivity (Fig. 4, 5), and reduced inhibition of hippocampal neuronal excitability (Fig. 6). The M518V mutation also accelerated degradation by ubiquitination as well as neuronal injury and death (Fig. 7–8).

Pathogenetic effects of M518V mutation at CaM contact site of $K_v7.2$ helix B

The *de novo* M518V mutation was found in a boy who displayed drug-resistant neonatal tonic-clonic seizures, and later developed profound mental retardation, speech impairment, spasticity, and autism (Weckhuysen et al., 2012). In this study, we demonstrate that M518V mutation induced multiple defects in K_v7 channels. The M518V mutation located at the CaM N-lobe contact site in helix B severely reduced CaM binding to $K_v7.2$ (Fig. 1, 2) and surface expression of heteromeric $K_v7.2$/ $K_v7.3$ channels in distal axons (Fig. 3). M518 and R525 residues are critical residues that mediate electrostatic interaction with CaM N-lobe (Xu et al., 2013). Considering that BFNE mutation R525Q disrupts CaM interaction with $K_v7.2$ (Ambrosino et al., 2015), M518V mutation may primarily impair the electrostatic association between $K_v7.2$ and CaM N-lobe (Strulovich et al., 2016; Xu et al., 2013) by disrupting hydrophobic packing at the interface between $K_v7.2$ and CaM N-lobe (Fig. 1D). Consistent with previous studies in Xenopus oocyte by Maljevic and colleagues (Orhan et

al., 2013), $K_v7.2$-M518V mutant channels displayed low level of K^+ currents in CHOhm1 cells, which were still larger than in GFP transfected control cells, and enough to modestly hyperpolarize resting membrane potentials (Fig. 4, Table 1). Considering the crucial roles of CaM binding to $K_v7.2$ for polarized axonal surface expression, K_v7 channel conductance, and inhibition of hippocampal neuronal excitability (Cavaretta et al., 2014; Shahidullah et al., 2005), a severe reduction of CaM binding serves as one major pathogenic mechanism underlying the M518V mutation.

One unexpected effect of the M518V mutation is ubiquitination and accelerated proteasome-dependent degradation of $K_v7.2$ when expressed alone (Fig. 7), indicative of ER-associated degradation (Ellgaard and Helenius, 2003). Although CaM binding was severely reduced by A343D mutation in the CaM contact site of helix A and M518V mutation in the CaM contact site of helix B (Fig. 2), no significant ubiquitination was found in $K_v7.2$-A343D proteins. we speculate that disruption of helix B structure and subsequent loss of CaM binding to helix B by M518V mutation (Fig. 1–2) may reveal a unique misfolded conformation that can be recognized by ubiquitin ligases. Previous studies have shown that a BFNE frameshift mutation creates a novel proteasomal degradation signal RCXRG in $K_v7.2$ (Soldovieri et al., 2006; Su et al., 2011). Furthermore, ubiquitination of $K_v7.3$ on XPXPPY motif by the E3 ubiquitin ligase Nedd4–2 has been reported to decrease surface and current expression of $K_v7.3$-containing channels (Ekberg et al., 2007). Although the amino acid sequence surrounding M518V mutation does not conform to either RCXRG or XPXPPY motif, it is possible that M518V mutation itself may provide a novel ubiquitination signal. Since coexpression of $K_v7.3$ increased expression of $K_v7.2$-M518V proteins (Fig. 8, S7), $K_v7.3$ binding to $K_v7.2$-M518V may most likely hinder the recognition of ubiquitinated $K_v7.2$-M518V by the proteasome. Understanding the molecular mechanisms underlying ubiquitination and degradation of $K_v7.2$-M518V warrants future studies.

Misfolded proteins can perturb normal cellular functions and lead to cytotoxicity when the cells fail to perform chaperone-assisted refolding, ubiquitin-proteasome mediated degradation, or aggresome-autophagy dependent clearance of these proteins (Su et al., 2011; Tyedmers et al., 2010). Indeed, we were surprised to find that a large fraction of HEK293T cells transfected with $K_v7.2$-M518V alone displayed cell shrinkage and nuclear condensation, indicative of apoptosis (Fig. 8). Similarly, expression of $K_v7.2$-M518V alone or together with $K_v7.3$ in hippocampal neurons increased neurite fragmentation and the loss of ankyrin-G at the AIS (Fig. 8). Although intracellular deposits of ubiquitinated proteins have been found in neurons affected by multiple neurodegenerative diseases (Dantuma and Bott, 2014) and Dravet Syndrome (Kang et al., 2015), this study is the first to introduce neuronal injury as a possible pathogenic mechanism for $K_v7.2$ epileptic encephalopathy (Fig. 9).

It is unclear how expression of $K_v7.2$-M518V causes cell death. Transfection of $K_v7.2$-M518V alone increased cell death in HEK293T cells and hippocampal neurons (Fig. 8), suggesting that ubiquitination and accelerated degradation of $K_v7.2$-M518V may contribute to cell death. Previous studies reported that disruption of the ubiquitin-proteasome system leads to cell cycle disruption and programmed cell death (Bence et al., 2001; Ross and Poirier, 2005). Although misfolded $K_v7.2$-M518V proteins are initially degraded by the

ubiquitin-proteasome system (Fig. 7), it is possible that failure of chaperone-assisted refolding and continuous production of misfolded K_v7.2-M518V proteins could saturate the capacity of the ER and proteasome, leading to ER stress, proteasome inhibition, and activation of apoptosis (Su et al., 2011; Tyedmers et al., 2010). Prevention of degradation by K_v7.3 (Fig. 8, S7) may further aggravate this situation by accumulating ubiquitinated K_v7.2-M518V proteins. Importantly, increased ER stress response has also been detected in the brains of human patients with temporal lobe epilepsy (TLE) and acute induction of seizures in rodent models of TLE (Engel et al., 2013; Kitao et al., 2001; Yamamoto et al., 2006), which are associated with sclerosis and apoptosis at or near the seizure foci (Coan et al., 2014). Severe reduction in axonal surface expression and current expression of K_v7.2-M518V-containing channels (Fig. 3–4) is expected to increase excitability of neurons compared to those expressing wild-type K_v7.2. Though highly speculative, such neuronal hyperexcitability induced by K_v7.2-M518V may further enhance the ER stress and apoptosis in addition to activating excitotoxicity.

The effects of K_v7.2-M518V expression on neuronal death and injury is particularly interesting since the brain magnetic resonance imaging (MRI) study of a patient with the M518V mutation shows substantial brain lesions and neuronal loss indicated by small frontal lobes, thinned splenium of corpus callosum, ventriculomegaly, and increased cerebral spinal fluid space (Weckhuysen et al., 2012). Neuronal death induced by K_v7.2-M518V accumulation may subsequently facilitate reorganization of circuits that results in hyperexcitability and seizures. In support of this notion, genetic inactivation of autophagy prevents the clearance of aggregated misfolded ubiquitinated proteins and causes neurodegeneration and spontaneous seizures in mice (Komatsu et al., 2006; McMahon et al., 2012), suggesting that epileptic seizures may arise as a consequence of abnormal accumulation of misfolded ubiquitinated proteins. An important task for future studies will be to dissect the molecular mechanisms underlying K_v7.2-M518V-mediated toxicity and its role in the etiology of epileptic encephalopathy.

Pathogenetic effects of R333W, K526N, and R532W mutations near CaM contact sites of K_v7.2 helices A and B

The R333W mutation was found in a boy who suffered from drug resistant seizures, Rolandic epilepsy, and psychomotor delay (Schmitt et al., 2005). The *de novo* R333W mutation was recently associated with intellectual disability and autism with high levels of recurrence (Geisheker et al., 2017). Our study is the first to characterize the effect of this mutation on CaM binding, expression, and function of K_v7.2. We found that the R333W mutation located proximal to the CaM C-lobe contact site in helix A reduced axonal surface expression of heteromeric channels by 30% (Fig. 3), consistent with its modest effect on reducing apoCaM binding to K_v7.2 (Fig. 2). Furthermore, K_v7.2-R333W channels displayed insensitivity to PIP_2 despite normal voltage-dependent activation (Fig. 4–5). Importantly, the R333W mutation blocked the ability of K_v7 channels to inhibit hippocampal neuronal excitability (Fig. 6) without affecting channel assembly (Fig. 2). Methylation of R333 has been recently reported to enhance K_v7.2 binding to PIP_2 (Kim et al., 2016), further implicating R333 as a critical residue for gating modulation by PIP_2. Considering the crucial roles of CaM binding to K_v7.2 in M-current expression and inhibition of hippocampal

neuronal excitability (Shahidullah et al., 2005), a combination of reduced binding of CaM and PIP_2 to $K_v7.2$ as well as decreased axonal expression of heteromeric channels may underlie the inability of $K_v7.2$-R333W containing channels to suppress excitability in hippocampal neurons (Fig. 6).

The K526N mutation was found in all affected members in a BFNE family, who exhibited BFNE alone or together with severe epileptic encephalopathy that displayed drug-resistant seizures, mental retardation, white matter reduction, and enlarged lateral ventricles (Borgatti et al., 2004). Here, we show that K526N mutation located distal to the CaM N-lobe contact site in helix B caused a 30% reduction in axonal surface expression of heteromeric channels but did not significantly decrease $K_v7.2$ binding to apoCaM and $K_v7.3$ (Fig. 1–3). The K526N mutation induced a modest right shift in voltage-dependence of $K_v7.2$ channels without altering peak current densities in CHO hm1 cells (Fig. 4–5). A previous study by Borgatti et al reported a right shift in voltage-dependence of homomeric $K_v7.2$-K526N channels in CHO cells (Borgatti et al., 2004). The difference in voltage-dependence is unclear, but could be attributed to the use of different CHO cell lines. While Borgatti et al used CHO cells, we used CHO hm1 cells which stably express human muscarinic receptors (Kosenko et al., 2012). Another unexpected result was that the K526N mutation enhanced PIP_2 sensitivity in CHO hm1 cells (Fig. 5). The PIP_2 concentration is estimated to be 10 μM and in the range of 1–3% of total lipid (McLaughlin et al., 2002; van den Bogaart et al., 2011), which is much lower than the saturating concentration of diC8-PIP_2 used in this study. Although soluble diC8-PIP_2 will partition between the aqueous and membrane lipid phases, diC8-PIP_2 has a lower effective concentration in the membrane than in the pipette solution (Collins and Gordon, 2013). Furthermore, mice lacking a single copy of the *Kcnq2* gene display increased susceptibility to convulsant agents (Watanabe et al., 2000). Therefore, the 30% reduction of axonal K_v7 channels by the K526N mutation, rather than increased PIP_2 sensitivity, may be sufficient to block their function in dampening hippocampal neuronal excitability (Fig. 6). It is also possible that this mutation may impair critical roles of K_v7 in mediating medium afterhyperpolarization (Tzingounis and Nicoll, 2008) or disrupt regulation of K_v7 channels by other signaling proteins including AKAP79/150 and syntaxin1A (Delmas and Brown, 2005; Etzioni et al., 2011; Hernandez et al., 2008; Hoshi et al., 2005; Hoshi et al., 2003; Regev et al., 2009; Suh and Hille, 2002; Suh and Hille, 2007).

Although the R532W mutation is located in the linker between helix B that mediates CaM binding (Alaimo et al., 2012; Gamper and Shapiro, 2003; Xu et al., 2013; Yus-Najera et al., 2002) and helix C that mediates subunit interaction (Schwake et al., 2006), this mutation did not alter $K_v7.2$ binding to apoCaM or $K_v7.3$ (Fig. 2). Instead, this mutation decreased axonal surface expression by 30% (Fig. 3). Furthermore, R532W mutation decreased K^+ current density of $K_v7.2$ channels by half, right-shifted their voltage-dependence, slowed their activation kinetics, and impaired their gating modulation by PIP_2 (Fig. 4–5). Remarkably, expression of $K_v7.2$-R532W resulted in hyperexcitability in hippocampal neurons (Fig. 6), suggesting that this mutant subunit may dominantly suppress channel function upon forming heteromeric channels with endogenous $K_v7.3$. These multiple defects in K_v7 channels and subsequent neuronal hyperexcitability may underlie the etiology of *de novo* R532W mutation associated with drug-resistant neonatal tonic-clonic seizures, profound mental

retardation, speech impairment, severe spastic quadriplegia, and mild microcephaly (Weckhuysen et al., 2012).

Implication of PIP_2 modulation residues near CaM contact sites in $K_V7.2$ helices A and B.

In the C-terminal tail of $K_V7.1$, PIP_2 has been reported to bind basic residues K354, K358, R360, and K362 in prehelix A (Thomas et al., 2011) and K526 and K527 in helix B (Tobelaim et al., 2017b). Consistently, introduction of mutations in these residues decreases PIP_2 interaction with the $K_V7.1$ C-terminal tail *in vitro* and gating modulation by PIP_2 (Thomas et al., 2011; Tobelaim et al., 2017b). In the cryo-EM structure of homomeric Xenopus $K_V7.1$, residues K526, K527, and K528 in $K_V7.1$ are well positioned near the membrane to interact with phospholipid head groups (Sun and MacKinnon, 2017). In $K_V7.2$ helix B distal to the CaM contact site, a cluster of basic residues (K524, R525, and K526 in protein accession CAA 75348.1) are structurally located close to the beginning of helix A where another cluster of positively charged basic residues (R325, K331, R332, and R333) are located (Fig. 1C). These positively charged residues in proximal helix A and distal helix B may constitute the site for PIP_2 modulation. This possibility is strongly supported by a previous report demonstrating reduced PIP_2 modulation of $K_V7.2$-R325G channels (Soldovieri et al., 2016), and by our findings that K526N enhanced whereas R333W reduced PIP_2 sensitivity of $K_V7.2$ channels (Fig. 5). Considering that $K_V7.1$-K528N proteins retain PIP_2 interaction to a similar extent as wild type $K_V7.1$ (Tobelaim et al., 2017b), increased PIP_2 sensitivity of $K_V7.2$-K526N channels may be caused by local conformational change. Our demonstration of PIP_2-insensitive $K_V7.2$-R532W channels (Fig. 5) not only reveal R532 as a novel PIP_2 interacting residue, but also suggests the helix B-C linker is another possible region that mediates PIP_2 sensitivity.

The proximity of PIP_2 and CaM binding sites raises an interesting possibility that coordinated actions of PIP_2 and CaM may regulate function and axonal surface expression of K_V7 channels. Competitive binding of PIP_2 and Ca^{2+}-bound CaM to helix B has been recently demonstrated in $K_V7.1$ and $K_V7.2$ (Tobelaim et al., 2017a; Tobelaim et al., 2017b). However, current density of wild type $K_V7.2$ channels but not PIP_2-insensitive $K_V7.2$-R325G channels can be enhanced by coexpression of CaM or CaM1234 that cannot bind to Ca^{2+} (Ambrosino et al., 2015; Soldovieri et al., 2016), suggesting that both apoCaM and Ca^{2+}-bound CaM may enhance current by increasing PIP_2 binding to $K_V7.2$ (Alberdi et al., 2015; Kosenko and Hoshi, 2013). Though highly speculative, we propose that PIP_2 binds a composite site formed by both CaM lobes and residues in $K_V7.2$ helices A and B.

Revisiting the role of CaM binding in polarized axonal surface expression of K_V7 channels.

While the A343D mutation in the IQ motif of helix A abolished apoCaM binding to $K_V7.2$ and axonal surface expression of heteromeric K_V7 channels (Fig. 2) (Cavaretta et al., 2014), the R333W mutation located proximal to the IQ motif in helix A modestly decreased apoCaM binding to $K_V7.2$ by 20% (Fig. 2) and reduced axonal surface expression of heteromeric channels by 30% (Fig. 3). In contrast to A343D mutation, the M518V mutation located at the CaM contact site in $K_V7.2$ helix B severely reduced apoCaM binding to $K_V7.2$ by 85% (Fig. 2) and surface expression of heteromeric channels in distal axons (Fig. 3). CaM binds to the antiparallel coiled-coil architecture of helices A and B of $K_V7.2$ with helix

A binding to CaM C-lobe, and helix B interacting with the CaM N-lobe (Strulovich et al., 2016; Xu et al., 2013; Yus-Najera et al., 2002). Therefore, disruption of helix B interaction with the CaM N-lobe severely compromises helix A binding to CaM C-lobe. The residual interaction between apoCaM and K_v7.2-M518V through helix A (Fig. 2) could account for the low surface expression of heteromeric K_v7.3/K_v7.2-M518V channels at the AIS (Fig. 3). Since none of these mutations affected subunit interaction (Fig.3), these results together suggest that helix A provides a dominant interaction site for apoCaM that promotes trafficking of heteromeric channels from the ER to the axonal surface and that the degree of apoCaM binding to K_v7.2 helix A governs the amount of axonal K_v7 channels on the neuronal plasma membrane.

Surprisingly, the K526N mutation located distal to the CaM N-lobe contact site in helix B decreased axonal surface expression of heteromeric channels by 30%, although the observed 35% reduction in bound apoCaM did not reach statistical significance (Fig. 1–2). This result was unexpected because CaM binding to the K_v7.2 C-terminal tail is significantly reduced by BFNE mutation R525Q (Ambrosino et al., 2015), which immediately precedes K526. In addition, the R532W mutation in the helix B-C linker also decreased axonal surface expression by 30% (Fig. 3) without altering K_v7.2 binding to apoCaM or K_v7.3 (Fig. 1–2). It is unclear how K526N and R532W mutations modestly decreased axonal surface expression of K_v7 channels without significantly reducing K_v7.2 interaction with CaM or K_v7.3. We have previously shown that axonal surface expression of K_v7 channels can be reduced by 30% upon coexpression of CaM1234, which cannot bind to Ca^{2+} (Cavaretta et al., 2014), suggesting that Ca^{2+}-bound CaM can further enhance channel targeting to the axonal surface. Considering that Ca^{2+}-bound CaM favors interaction with helix B (Alaimo et al., 2012; Gamper and Shapiro, 2003; Xu et al., 2013; Yus-Najera et al., 2002), we speculate that K526N and R532W mutations may modestly decrease axonal surface expression of K_v7 channels by reducing K_v7.2 affinity to Ca^{2+}-bound CaM.

CONCLUSIONS

Here, we discovered molecular pathogenetic mechanisms for epileptic encephalopathy mutations in helices A and B and helix B-C linker of K_v7.2. These mutations cause a reduction in K_v7 polarized axonal surface expression and K_v7 function to inhibit neuronal excitability by variably decreasing CaM binding, voltage-dependent activation, and PIP_2 sensitivity (Fig. 9). One particular mutation M518V induced abnormal accumulation of ubiquitinated K_v7.2 in the presence of K_v7.3 and caused neuronal injury (Fig. 9), opening a new avenue for exploring therapeutic drugs that can alleviate accumulation of misfolded proteins. Since inhibition of K_v7 currents during early neonatal development induces hippocampal sclerosis in addition to increased seizure susceptibility (Peters et al., 2005), our discovery supports the critical importance in early identification of a mutation and its pathogenic mechanism in order to develop effective mutation-specific therapy to combat neuronal hyperexcitability and remediate neuronal injury associated with drug-refractory K_v7.2 epileptic encephalopathy.

Supplementary Material

Refer to Web version on PubMed Central for supplementary material.

ACKNOWLEDGEMENTS

We thank Dr. Naoto Hoshi (UC Irvine) for providing CHOhm1 cells and Amanda Weiss for her technical assistance with neuronal culture. This research was supported by the Research Project Grant #R01NS083402 from the NIH National institute of Neurological Disorders and Stroke (PI: Chung), Carver Young Investigator Grant Award #11–38870 from Roy J. Carver Charitable Trust (PI: Chung), Targeted Research Initiative for Severe Symptomatic Epilepsies Grant #C4107 from Epilepsy Foundation (PI: Chung).

ABBREVIATIONS

CaM	calmodulin
K^+	potassium
AP	action potential
AIS	axonal initial segments
BFNE	benign familial neonatal epilepsy
EEG	electroencephalogram
PIP_2	phosphatidylinositol 4,5-bisphosphate
AKAP	A-kinase-anchoring protein
ER	endoplasmic reticulum
YFP	yellow fluorescent protein
TLE	temporal lobe epilepsy

REFERENCES

Abidi A, et al., 2015 A recurrent KCNQ2 pore mutation causing early onset epileptic encephalopathy has a moderate effect on M current but alters subcellular localization of Kv7 channels. Neurobiol Dis. 80, 80–92. [PubMed: 26007637]

Alaimo A, et al., 2012 Cooperativity between calmodulin binding sites in Kv7.2 channels. J Cell Sci.

Alaimo A, et al., 2009 Calmodulin activation limits the rate of KCNQ2 K+ channel exit from the endoplasmic reticulum. J Biol Chem. 284, 20668–75. [PubMed: 19494108]

Alberdi A, et al., 2015 Uncoupling PIP2-calmodulin regulation of Kv7.2 channels by an assembly destabilizing epileptogenic mutation. J Cell Sci. 128, 4014–23. [PubMed: 26359296]

Ambrosino P, et al., 2015 Epilepsy-causing mutations in Kv7.2 C-terminus affect binding and functional modulation by calmodulin. Biochim Biophys Acta. 1852, 1856–66. [PubMed: 26073431]

Bence NF, et al., 2001 Impairment of the ubiquitin-proteasome system by protein aggregation. Science. 292, 1552–5. [PubMed: 11375494]

Bennett V, Lorenzo DN, 2016 An Adaptable Spectrin/Ankyrin-Based Mechanism for Long-Range Organization of Plasma Membranes in Vertebrate Tissues. Curr Top Membr. 77, 143–84. [PubMed: 26781832]

Biervert C, et al., 1998 A potassium channel mutation in neonatal human epilepsy. Science. 279, 403–6. [PubMed: 9430594]

Blackburn-Munro G, et al., 2005 Retigabine: chemical synthesis to clinical application. CNS Drug Rev. 11, 1–20. [PubMed: 15867950]

Borgatti R, et al., 2004 A novel mutation in KCNQ2 associated with BFNC, drug resistant epilepsy, and mental retardation. Neurology. 63, 57–65. [PubMed: 15249611]

Bortner CD, Cidlowski JA, 2002 Apoptotic volume decrease and the incredible shrinking cell. Cell Death Differ. 9, 1307–10. [PubMed: 12478467]

Brown DA, Passmore GM, 2009 Neural KCNQ (Kv7) channels. Br J Pharmacol. 156, 1185–95. [PubMed: 19298256]

Cavaretta JP, et al., 2014 Polarized Axonal Surface Expression of Neuronal KCNQ Potassium Channels Is Regulated by Calmodulin Interaction with KCNQ2 Subunit. PLoS One. 9, e103655. [PubMed: 25077630]

Charlier C, et al., 1998 A pore mutation in a novel KQT-like potassium channel gene in an idiopathic epilepsy family. Nat Genet. 18, 53–5. [PubMed: 9425900]

Chung HJ, 2014 Role of calmodulin in neuronal Kv7/KCNQ potassium channels and epilepsy. . Frontiers in Biology. 9, 205–215.

Chung HJ, et al., 2006 Polarized axonal surface expression of neuronal KCNQ channels is mediated by multiple signals in the KCNQ2 and KCNQ3 C-terminal domains. Proc Natl Acad Sci U S A. 103, 8870–5. [PubMed: 16735477]

Clark BD, et al., 2009 Electrogenic tuning of the axon initial segment. Neuroscientist. 15, 651–68. [PubMed: 20007821]

Coan AC, et al., 2014 Frequent seizures are associated with a network of gray matter atrophy in temporal lobe epilepsy with or without hippocampal sclerosis. PLoS One. 9, e85843. [PubMed: 24475055]

Collins MD, Gordon SE, 2013 Short-chain phosphoinositide partitioning into plasma membrane models. Biophys J. 105, 2485–94. [PubMed: 24314079]

Cooper EC, et al., 2001 M channel KCNQ2 subunits are localized to key sites for control of neuronal network oscillations and synchronization in mouse brain. J Neurosci. 21, 9529–40. [PubMed: 11739564]

Dantuma NP, Bott LC, 2014 The ubiquitin-proteasome system in neurodegenerative diseases: precipitating factor, yet part of the solution. Front Mol Neurosci. 7, 70. [PubMed: 25132814]

Dedek K, et al., 2003 Neonatal convulsions and epileptic encephalopathy in an Italian family with a missense mutation in the fifth transmembrane region of KCNQ2. Epilepsy Res. 54, 21–7. [PubMed: 12742592]

Dedek K, et al., 2001 Myokymia and neonatal epilepsy caused by a mutation in the voltage sensor of the KCNQ2 K+ channel. Proc Natl Acad Sci U S A. 98, 12272–7. [PubMed: 11572947]

Delmas P, Brown DA, 2005 Pathways modulating neural KCNQ/M (Kv7) potassium channels. Nat Rev Neurosci. 6, 850–62. [PubMed: 16261179]

Ekberg J, et al., 2007 Regulation of the voltage-gated K(+) channels KCNQ2/3 and KCNQ3/5 by ubiquitination. Novel role for Nedd4–2. J Biol Chem. 282, 12135–42. [PubMed: 17322297]

Ellgaard L, Helenius A, 2003 Quality control in the endoplasmic reticulum. Nat Rev Mol Cell Biol. 4, 181–91. [PubMed: 12612637]

Engel T, et al., 2013 CHOP regulates the p53-MDM2 axis and is required for neuronal survival after seizures. Brain. 136, 577–92. [PubMed: 23361066]

Etxeberria A, et al., 2008 Calmodulin regulates the trafficking of KCNQ2 potassium channels. FASEB J. 22, 1135–43. [PubMed: 17993630]

Etzioni A, et al., 2011 Regulation of neuronal M-channel gating in an isoform-specific manner: functional interplay between calmodulin and syntaxin 1A. J Neurosci. 31, 14158–71. [PubMed: 21976501]

Fisher RS, et al., 2005 Epileptic seizures and epilepsy: definitions proposed by the International League Against Epilepsy (ILAE) and the International Bureau for Epilepsy (IBE). Epilepsia. 46, 470–2. [PubMed: 15816939]

Gamper N, Shapiro MS, 2003 Calmodulin mediates Ca2+-dependent modulation of M-type K+ channels. J Gen Physiol. 122, 17–31. [PubMed: 12810850]

Gamper N, Shapiro MS, 2007 Target-specific PIP(2) signalling: how might it work? J Physiol. 582, 967–75. [PubMed: 17412762]

Gamper N, et al., 2005 The use of Chinese hamster ovary (CHO) cells in the study of ion channels. J Pharmacol Toxicol Methods. 51, 177–85. [PubMed: 15862463]

Geiger J, et al., 2006 Immunohistochemical analysis of KCNQ3 potassium channels in mouse brain. Neurosci Lett.

Geisheker MR, et al., 2017 Hotspots of missense mutation identify neurodevelopmental disorder genes and functional domains. Nat Neurosci. 20, 1043–1051. [PubMed: 28628100]

Gu N, et al., 2005 Kv7/KCNQ/M and HCN/h, but not KCa2/SK channels, contribute to the somatic medium after-hyperpolarization and excitability control in CA1 hippocampal pyramidal cells. J Physiol. 566, 689–715. [PubMed: 15890705]

Guerrini R, Noebels J, 2014 How can advances in epilepsy genetics lead to better treatments and cures? Adv Exp Med Biol. 813, 309–17. [PubMed: 25012387]

Gunthorpe MJ, et al., 2012 The mechanism of action of retigabine (ezogabine), a first-in-class K+ channel opener for the treatment of epilepsy. Epilepsia. 53, 412–24. [PubMed: 22220513]

Haitin Y, Attali B, 2008 The C-terminus of Kv7 channels: a multifunctional module. J Physiol. 586, 1803–10. [PubMed: 18218681]

Hernandez CC, et al., 2008 A carboxy-terminal inter-helix linker as the site of phosphatidylinositol 4,5-bisphosphate action on Kv7 (M-type) K+ channels. J Gen Physiol. 132, 361–81. [PubMed: 18725531]

Hoshi N, et al., 2005 Distinct enzyme combinations in AKAP signalling complexes permit functional diversity. Nat Cell Biol. 7, 1066–73. [PubMed: 16228013]

Hoshi N, et al., 2003 AKAP150 signaling complex promotes suppression of the M-current by muscarinic agonists. Nat Neurosci. 6, 564–71. [PubMed: 12754513]

Jaeger PA, Wyss-Coray T, 2009 All-you-can-eat: autophagy in neurodegeneration and neuroprotection. Mol Neurodegener. 4, 16. [PubMed: 19348680]

Jenkins PM, et al., 2015 Giant ankyrin-G: a critical innovation in vertebrate evolution of fast and integrated neuronal signaling. Proc Natl Acad Sci U S A. 112, 957–64. [PubMed: 25552556]

Jentsch TJ, 2000 Neuronal KCNQ potassium channels: physiology and role in disease. Nat Rev Neurosci. 1, 21–30. [PubMed: 11252765]

Kang JQ, et al., 2015 The human epilepsy mutation GABRG2(Q390X) causes chronic subunit accumulation and neurodegeneration. Nat Neurosci. 18, 988–96. [PubMed: 26005849]

Kato M, et al., 2013 Clinical spectrum of early onset epileptic encephalopathies caused by KCNQ2 mutation. Epilepsia. 54, 1282–7. [PubMed: 23621294]

Kim HJ, et al., 2016 Protein arginine methylation facilitates KCNQ channel-PIP2 interaction leading to seizure suppression. Elife. 5.

Kitao Y, et al., 2001 Expression of the endoplasmic reticulum molecular chaperone (ORP150) rescues hippocampal neurons from glutamate toxicity. J Clin Invest. 108, 1439–50. [PubMed: 11714735]

Komatsu M, et al., 2006 Loss of autophagy in the central nervous system causes neurodegeneration in mice. Nature. 441, 880–4. [PubMed: 16625205]

Kosenko A, Hoshi N, 2013 A change in configuration of the calmodulin-KCNQ channel complex underlies Ca2+-dependent modulation of KCNQ channel activity. PLoS One. 8, e82290. [PubMed: 24349250]

Kosenko A, et al., 2012 Coordinated signal integration at the M-type potassium channel upon muscarinic stimulation. EMBO J. 31, 3147–56. [PubMed: 22643219]

Kwong AK, et al., 2015 Analysis of mutations in 7 genes associated with neuronal excitability and synaptic transmission in a cohort of children with non-syndromic infantile epileptic encephalopathy. PLoS One. 10, e0126446. [PubMed: 25951140]

Large CH, et al., 2012 The spectrum of anticonvulsant efficacy of retigabine (ezogabine) in animal models: implications for clinical use. Epilepsia. 53, 425–36. [PubMed: 22221318]

Leaver-Fay A, et al., 2011 ROSETTA3: an object-oriented software suite for the simulation and design of macromolecules. Methods Enzymol. 487, 545–74. [PubMed: 21187238]

Lee KY, Chung HJ, 2014 NMDA receptors and L-type voltage-gated Ca(2)(+) channels mediate the expression of bidirectional homeostatic intrinsic plasticity in cultured hippocampal neurons. Neuroscience. 277, 610–23. [PubMed: 25086314]

Lee KY, et al., 2015 N-methyl-D-aspartate receptors mediate activity-dependent down-regulation of potassium channel genes during the expression of homeostatic intrinsic plasticity. Mol Brain. 8, 4. [PubMed: 25599691]

Logothetis DE, et al., 2015 Phosphoinositide control of membrane protein function: a frontier led by studies on ion channels. Annu Rev Physiol. 77, 81–104. [PubMed: 25293526]

Maeno E, et al., 2000 Normotonic cell shrinkage because of disordered volume regulation is an early prerequisite to apoptosis. Proc Natl Acad Sci U S A. 97, 9487–92. [PubMed: 10900263]

Maljevic S, Lerche H, 2014 Potassium channel genes and benign familial neonatal epilepsy. Prog Brain Res. 213, 17–53. [PubMed: 25194482]

McLaughlin S, et al., 2002 PIP(2) and proteins: interactions, organization, and information flow. Annu Rev Biophys Biomol Struct. 31, 151–75. [PubMed: 11988466]

McMahon J, et al., 2012 Impaired autophagy in neurons after disinhibition of mammalian target of rapamycin and its contribution to epileptogenesis. J Neurosci. 32, 15704–14. [PubMed: 23136410]

Miceli F, et al., 2015 Early-onset epileptic encephalopathy caused by gain-of-function mutations in the voltage sensor of Kv7.2 and Kv7.3 potassium channel subunits. J Neurosci. 35, 3782–93. [PubMed: 25740509]

Milh M, et al., 2013 Similar early characteristics but variable neurological outcome of patients with a de novo mutation of KCNQ2. Orphanet J Rare Dis. 8, 80. [PubMed: 23692823]

Millichap JJ, et al., 2016 KCNQ2 encephalopathy: Features, mutational hot spots, and ezogabine treatment of 11 patients. Neurol Genet. 2, e96. [PubMed: 27602407]

Numis AL, et al., 2014 KCNQ2 encephalopathy: delineation of the electroclinical phenotype and treatment response. Neurology. 82, 368–70. [PubMed: 24371303]

Orhan G, et al., 2013 Dominant-negative Effects of KCNQ2 Mutations are Associated with Epileptic Encephalopathy. Ann Neurol.

Pan Z, et al., 2006 A common ankyrin-G-based mechanism retains KCNQ and NaV channels at electrically active domains of the axon. J Neurosci. 26, 2599–613. [PubMed: 16525039]

Peters HC, et al., 2005 Conditional transgenic suppression of M channels in mouse brain reveals functions in neuronal excitability, resonance and behavior. Nat Neurosci. 8, 51–60. [PubMed: 15608631]

Psenka TM, Holden KR, 1996 Benign familial neonatal convulsions; psychosocial adjustment to the threat of recurrent seizures. Seizure. 5, 243–5. [PubMed: 8902929]

Rasmussen HB, et al., 2007 Requirement of subunit co-assembly and ankyrin-G for M-channel localization at the axon initial segment. J Cell Sci. 120, 953–63. [PubMed: 17311847]

Regev N, et al., 2009 Selective interaction of syntaxin 1A with KCNQ2: possible implications for specific modulation of presynaptic activity. PLoS One. 4, e6586. [PubMed: 19675672]

Ross CA, Poirier MA, 2005 Opinion: What is the role of protein aggregation in neurodegeneration? Nat Rev Mol Cell Biol. 6, 891–8. [PubMed: 16167052]

Sachyani D, et al., 2014 Structural basis of a Kv7.1 potassium channel gating module: studies of the intracellular c-terminal domain in complex with calmodulin. Structure. 22, 1582–94. [PubMed: 25441029]

Saitsu H, et al., 2012 Whole exome sequencing identifies KCNQ2 mutations in Ohtahara syndrome. Ann Neurol. 72, 298–300. [PubMed: 22926866]

Samanta D, et al., 2015 Myoclonic epilepsy evolved into West syndrome: a patient with a novel de novo KCNQ2 mutation. Acta Neurol Belg. 115, 475–8. [PubMed: 25092550]

Schafer DP, et al., 2009 Disruption of the axon initial segment cytoskeleton is a new mechanism for neuronal injury. J Neurosci. 29, 13242–54. [PubMed: 19846712]

Schmitt B, et al., 2005 Neonatal seizures with tonic clonic sequences and poor developmental outcome. Epilepsy Res. 65, 161–8. [PubMed: 16039833]

Schwake M, et al., 2006 Structural determinants of M-type KCNQ (Kv7) K+ channel assembly. J Neurosci. 26, 3757–66. [PubMed: 16597729]

Schwake M, et al., 2000 Surface expression and single channel properties of KCNQ2/KCNQ3, M-type K+ channels involved in epilepsy. J Biol Chem. 275, 13343–8. [PubMed: 10788442]

Schwarz JR, et al., 2006 KCNQ channels mediate IKs, a slow K+ current regulating excitability in the node of Ranvier. J Physiol.

Shah MM, et al., 2011 Differential effects of Kv7 (M-) channels on synaptic integration in distinct subcellular compartments of rat hippocampal pyramidal neurons. J Physiol. 589, 6029–38. [PubMed: 22041186]

Shah MM, et al., 2008 Functional significance of axonal Kv7 channels in hippocampal pyramidal neurons. Proc Natl Acad Sci U S A. 105, 7869–74. [PubMed: 18515424]

Shah MM, et al., 2002 Molecular correlates of the M-current in cultured rat hippocampal neurons. J Physiol. 544, 29–37. [PubMed: 12356878]

Shahidullah M, et al., 2005 Expression of a calmodulin-binding KCNQ2 potassium channel fragment modulates neuronal M-current and membrane excitability. Proc Natl Acad Sci U S A. 102, 16454–9. [PubMed: 16263935]

Singh NA, et al., 1998 A novel potassium channel gene, KCNQ2, is mutated in an inherited epilepsy of newborns. Nat Genet. 18, 25–9. [PubMed: 9425895]

Soh H, et al., 2014 Conditional deletions of epilepsy-associated KCNQ2 and KCNQ3 channels from cerebral cortex cause differential effects on neuronal excitability. J Neurosci. 34, 5311–21. [PubMed: 24719109]

Soldovieri MV, et al., 2016 Early-onset epileptic encephalopathy caused by a reduced sensitivity of Kv7.2 potassium channels to phosphatidylinositol 4,5-bisphosphate. Sci Rep. 6, 38167. [PubMed: 27905566]

Soldovieri MV, et al., 2006 Decreased subunit stability as a novel mechanism for potassium current impairment by a KCNQ2 C terminus mutation causing benign familial neonatal convulsions. J Biol Chem. 281, 418–28. [PubMed: 16260777]

Strulovich R, et al., 2016 Structural Insights into the M-Channel Proximal C-Terminus/Calmodulin Complex. Biochemistry. 55, 5353–65. [PubMed: 27564677]

Su J, et al., 2011 A novel degradation signal derived from distal C-terminal frameshift mutations of KCNQ2 protein which cause neonatal epilepsy. J Biol Chem. 286, 42949–58. [PubMed: 21937445]

Suh BC, Hille B, 2002 Recovery from muscarinic modulation of M current channels requires phosphatidylinositol 4,5-bisphosphate synthesis. Neuron. 35, 507–20. [PubMed: 12165472]

Suh BC, Hille B, 2007 Regulation of KCNQ channels by manipulation of phosphoinositides. J Physiol. 582, 911–6. [PubMed: 17412763]

Suh BC, et al., 2006 Rapid chemically induced changes of PtdIns(4,5)P2 gate KCNQ ion channels. Science. 314, 1454–7. [PubMed: 16990515]

Sun J, MacKinnon R, 2017 Cryo-EM Structure of a KCNQ1/CaM Complex Reveals Insights into Congenital Long QT Syndrome. Cell. 169, 1042–1050 e9. [PubMed: 28575668]

Thomas AM, et al., 2011 Characterization of a binding site for anionic phospholipids on KCNQ1. J Biol Chem. 286, 2088–100. [PubMed: 21084310]

Tobelaim WS, et al., 2017a Ca(2+)-Calmodulin and PIP2 interactions at the proximal C-terminus of Kv7 channels. Channels (Austin). 11, 686–695. [PubMed: 28976808]

Tobelaim WS, et al., 2017b Competition of calcified calmodulin N lobe and PIP2 to an LQT mutation site in Kv7.1 channel. Proc Natl Acad Sci U S A. 114, E869–E878. [PubMed: 28096388]

Tyedmers J, et al., 2010 Cellular strategies for controlling protein aggregation. Nat Rev Mol Cell Biol. 11, 777–88. [PubMed: 20944667]

Tzingounis AV, Nicoll RA, 2008 Contribution of KCNQ2 and KCNQ3 to the medium and slow afterhyperpolarization currents. Proc Natl Acad Sci U S A. 105, 19974–9. [PubMed: 19060215]

van den Bogaart G, et al., 2011 Membrane protein sequestering by ionic protein-lipid interactions. Nature. 479, 552–5. [PubMed: 22020284]

Wang HS, et al., 1998 KCNQ2 and KCNQ3 potassium channel subunits: molecular correlates of the M-channel. Science. 282, 1890–3. [PubMed: 9836639]

Watanabe H, et al., 2000 Disruption of the epilepsy KCNQ2 gene results in neural hyperexcitability. J Neurochem. 75, 28–33. [PubMed: 10854243]

Weber YG, et al., 2006 Immunohistochemical analysis of KCNQ2 potassium channels in adult and developing mouse brain. Brain Res.

Weckhuysen S, et al., 2013 Extending the KCNQ2 encephalopathy spectrum: clinical and neuroimaging findings in 17 patients. Neurology. 81, 1697–703. [PubMed: 24107868]

Weckhuysen S, et al., 2012 KCNQ2 encephalopathy: emerging phenotype of a neonatal epileptic encephalopathy. Ann Neurol. 71, 15–25. [PubMed: 22275249]

Wen H, Levitan IB, 2002 Calmodulin is an auxiliary subunit of KCNQ2/3 potassium channels. J Neurosci. 22, 7991–8001. [PubMed: 12223552]

Wuttke TV, et al., 2007 Peripheral nerve hyperexcitability due to dominant-negative KCNQ2 mutations. Neurology. 69, 2045–53. [PubMed: 17872363]

Xia XM, et al., 1998 Mechanism of calcium gating in small-conductance calcium-activated potassium channels. Nature. 395, 503–7. [PubMed: 9774106]

Xu Q, et al., 2013 Structure of a Ca(2+)/CaM:Kv7.4 (KCNQ4) B-helix complex provides insight into M current modulation. J Mol Biol. 425, 378–94. [PubMed: 23178170]

Yamamoto A, et al., 2006 Endoplasmic reticulum stress and apoptosis signaling in human temporal lobe epilepsy. J Neuropathol Exp Neurol. 65, 217–25. [PubMed: 16651883]

Yue C, Yaari Y, 2004 KCNQ/M channels control spike afterdepolarization and burst generation in hippocampal neurons. J Neurosci. 24, 4614–24. [PubMed: 15140933]

Yue C, Yaari Y, 2006 Axo-Somatic and Apical Dendritic Kv7/M Channels Differentially Regulate the Intrinsic Excitability of Adult Rat CA1 Pyramidal Cells. J Neurophysiol.

Yus-Najera E, et al., 2002 The identification and characterization of a noncontinuous calmodulin-binding site in noninactivating voltage-dependent KCNQ potassium channels. J Biol Chem. 277, 28545–53. [PubMed: 12032157]

Zhang Q, et al., 2016 Gene mutation analysis of 175 Chinese patients with early-onset epileptic encephalopathy. Clin Genet.

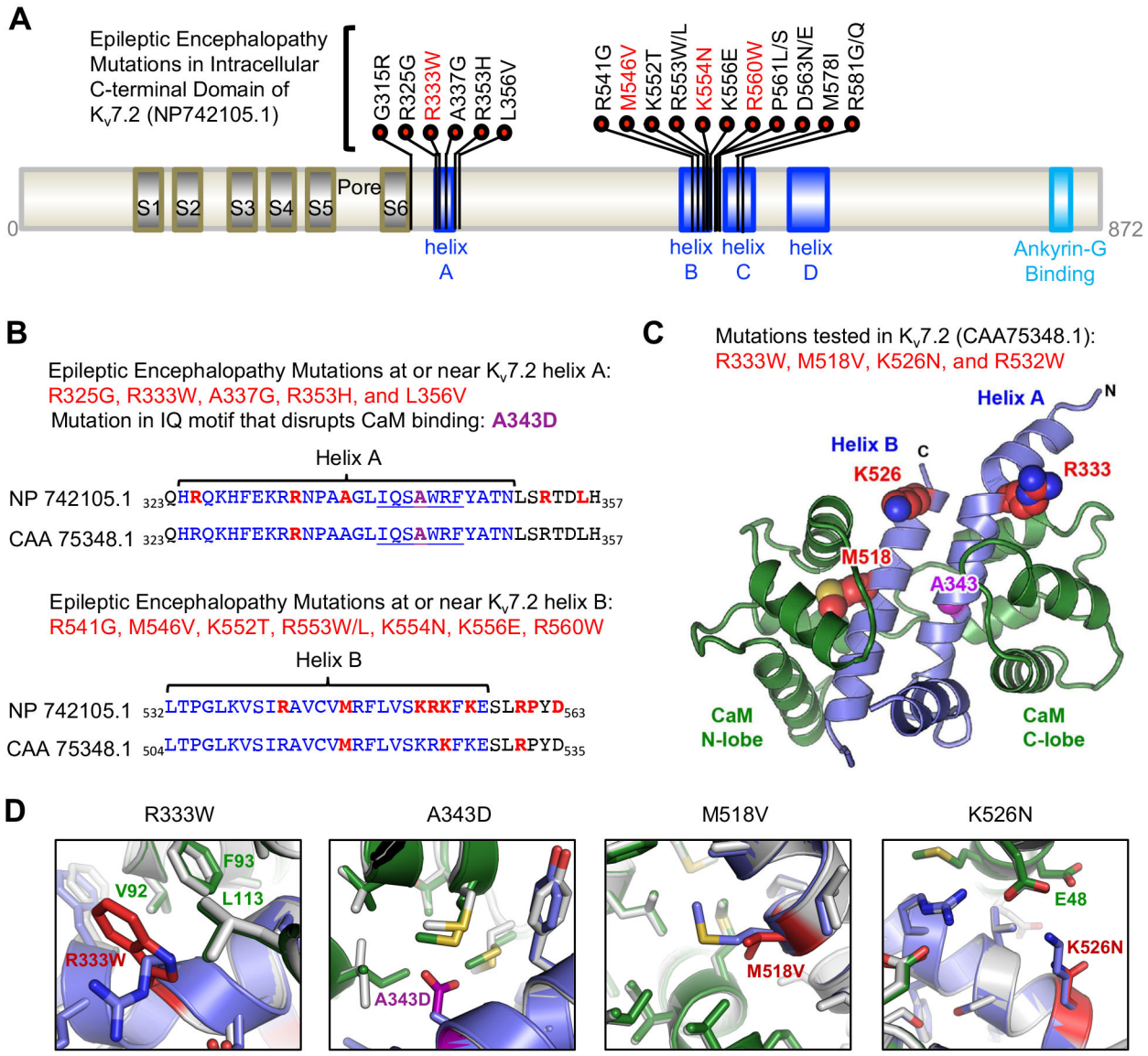

Figure 1. Distribution of epileptic encephalopathy mutations in CaM binding helices A and B of K_V7.2.

(A) K_V7.2 protein (NP_742105.1) showing functional domains including transmembrane S1–S6, a pore, an intracellular C-terminal tail containing helices A-D and ankyrin-G binding motif. Missense epileptic encephalopathy mutations are concentrated in helix A (residues 324–350), helix B (residues 532–557) and the linker between helix B and helix C (residues 568–589). The mutations (R333W, M546V, K554N) characterized in this study (red) are shown. **(B)** Amino acid sequence alignment of K_V7.2 (NP_742105.1) and a shorter K_V7.2 isoform (CAA_75348.1 used in this study) showing helices A and B (blue), CaM-binding consensus IQ motif in helix A (underlined), A343D mutation (purple), and epileptic encephalopathy mutations (red). **(C)** Amino acids (R333, M518, K526) mutated in epileptic encephalopathy and characterized in this study (red) are shown on a model of K_V7.2 helices A and B (blue) in complex with Ca^{2+}-bound CaM (green). A343 (purple) is located in helix A at the CaM C-lobe contact. R532 (not shown) is located distal to the helix B of this

structure. **(D)** The modeled structure of wild type $K_v7.2$ helix A-B (blue) bound to Ca^{2+}-bound CaM (green) is overlaid with the lowest energy model of the mutant $K_v7.2$ helix A-B (mutations in red) complexed with Ca^{2+}-bound CaM (grey).

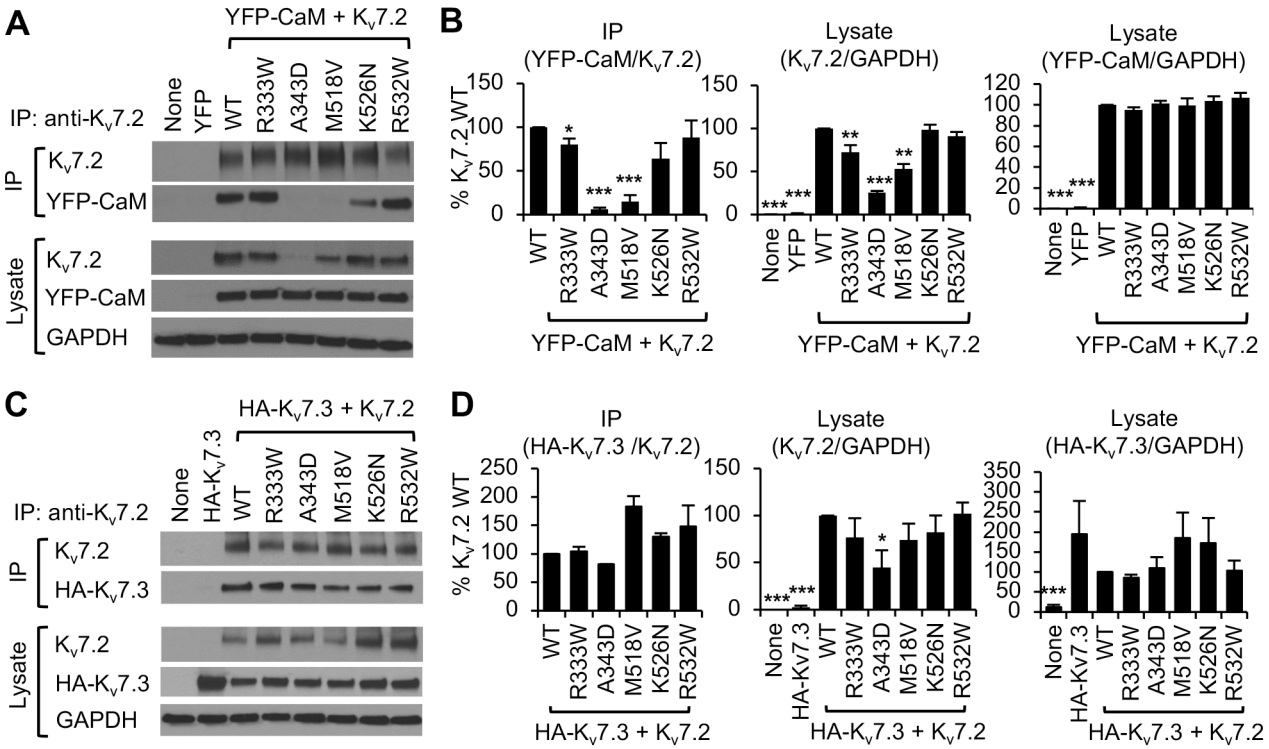

Figure 2. K_V7.2 expression and binding to apoCaM is impacted by epileptic encephalopathy mutations.

(A, B) Co-immunoprecipitation of YFP-CaM with wild type K_V7.2 (WT) or K_V7.2 containing epileptic encephalopathy mutations from transfected HEK283T cells. **(A)** Representative immunoblots. **(B)** Quantification of co-immunoprecipitation and lysate from 7 independent experiments: untransfected (None: n=6), YFP-CaM (n=6), YFP-CaM cotransfection with WT (n=7), R333W (n=7), A343D (n=6), M518V (n=7), K526N (n=6), or R532W (n=5). **(C, D)** Co-immunoprecipitation of K_V7.3 containing extracellular HA tag (HA-K_V7.3) with K_V7.2 WT or mutant K_V7.2 containing epileptic encephalopathy mutations from transfected HEK283T cells. **(C)** Representative immunoblots. **(D)** Quantification of co-immunoprecipitation and lysate from 6 independent experiments: untransfected cells (None: n=6), or cells transfected with HA-K_V7.3 (n=6), HA-K_V7.3 and K_V7.2 WT (n=6), R333W (n=6), A343D (n=4), M518V (n=5), K526N (n=5), or R532W (n=5). GAPDH served as a loading control. Data shown represent the Ave ± SEM (*p<0.05, **p<0.01, ***p<0.005).

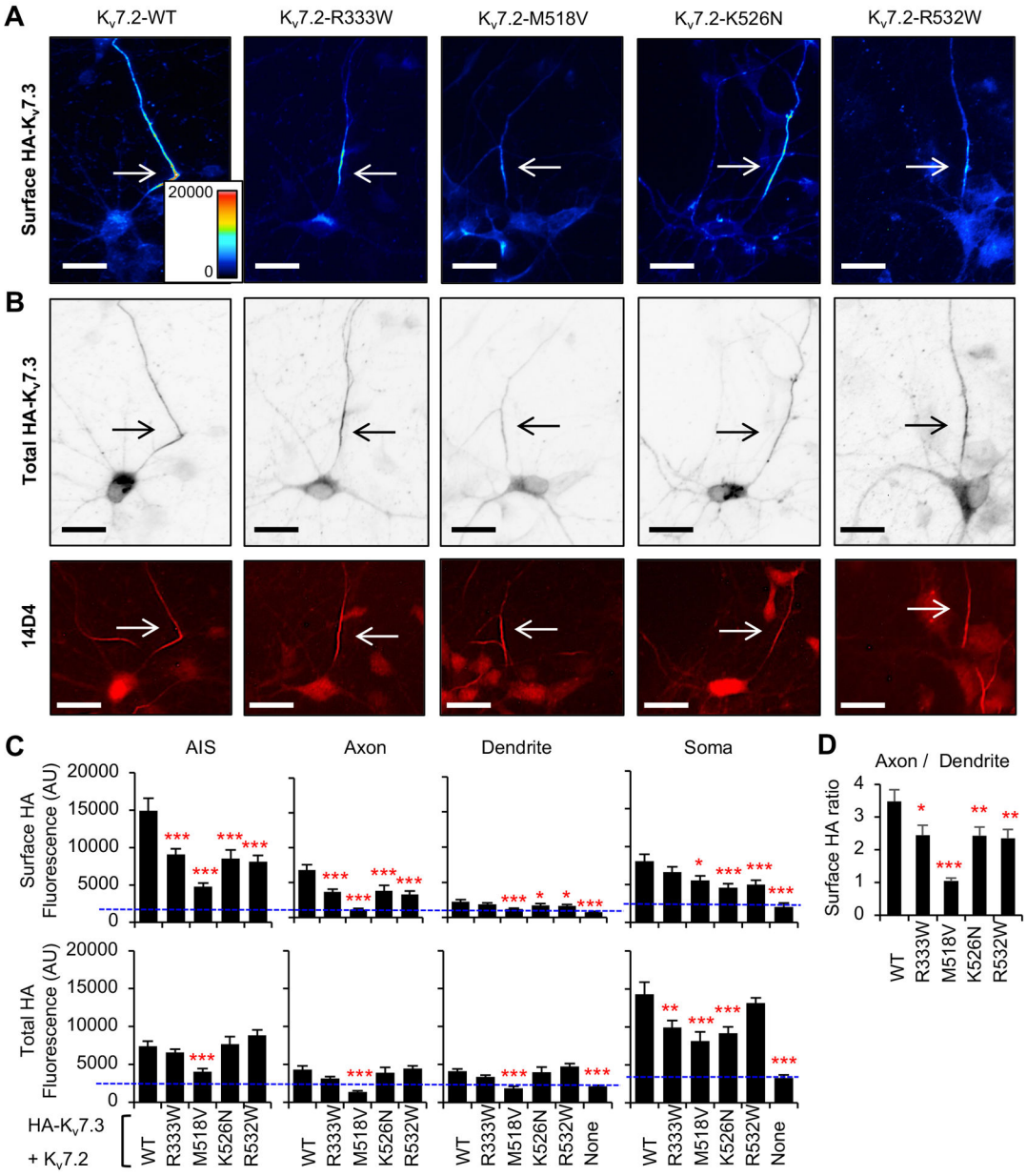

Figure 3. Polarized axonal surface expression of K_V7 channels is severely decreased M518V mutation, and modestly reduced by by R333W, K526N, and R532W mutations.

Immunocytochemistry showing surface and total HA-$K_V7.3$ proteins in hippocampal neurons cotransfected with $K_V7.2$ WT or $K_V7.2$ containing epileptic encephalopathy mutations. **(A)** Representative images of surface HA-$K_V7.3$ as pseudo-color that display differences in the surface HA intensities from high (red) to low (blue). **(B)** Representative images of total HA-$K_V7.3$ (*Upper-inverted gray*) and the axonal initial segments (AIS) identified by anti-phospho IκBα-Ser32 (14D4) antibodies (*Lower-fluorescence*) from the same neurons shown in (A). Arrows mark the AIS. Scale bars: 20 μm. **(C)** Background subtracted mean intensities of surface and total HA fluorescence from healthy neurons that were untransfected (None: n=20) or transfected with HA-$K_V7.3$ and $K_V7.2$ WT (n=36), R333W (n=35), M518V (n=22), K526N (n=39), or R532W (n=38) in 3 independent

experiments. AU, arbitrary unit. **(D)** Surface HA intensity ratio at distal axon over dendrite. Data shown represent the Ave ± SEM (*p<0.05, **p<0.01, ***p<0.005).

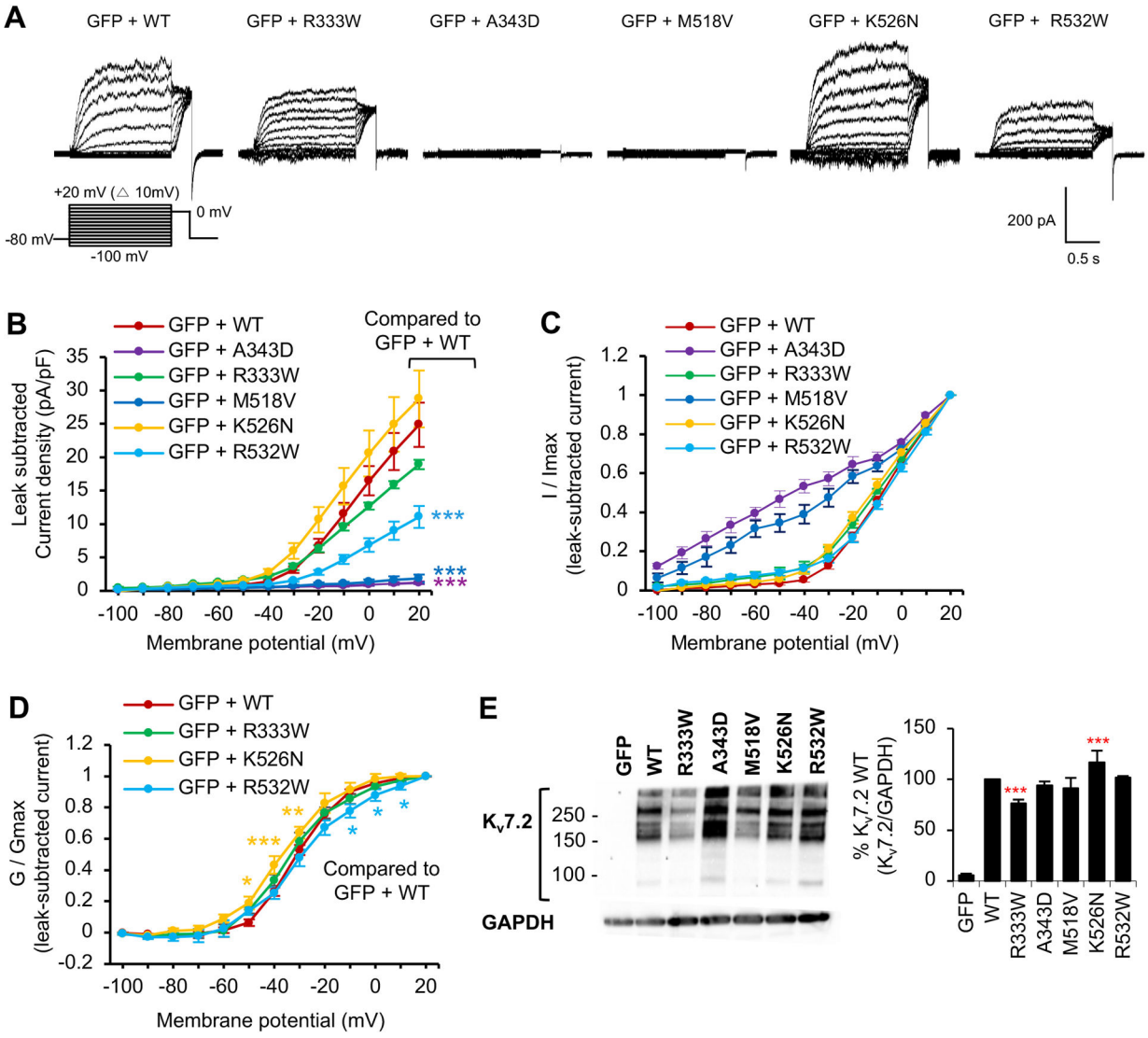

Figure 4. Voltage-dependent activation of $K_V7.2$ channels is decreased by R532W mutation and abolished by M518V mutation.

Whole cell voltage clamp recording of macroscopic K^+ currents from CHO hm1 cells transfected with GFP and $K_V7.2$ WT or $K_V7.2$ containing epileptic encephalopathy mutations. The cells were held at −80 mV. Currents were evoked by depolarization for 1.5 s from −100 mV to +20 mV in 10 mV increments, followed by a step to 0 mV for 300 ms. The raw current traces and data are shown in Supplemental Fig. 3. **(A)** Representative traces of currents from which leak currents were subtracted at all voltage steps. Leak current was defined as non-voltage-dependent current from GFP-transfected cells. **(B-D)** Average peak current densities (B), normalized currents (C), and normalized conductance (G / Gmax) (D) were quantified using leak subtracted currents at all voltage steps. The number of transfected cells that were analyzed: GFP (n=9), GFP and $K_V7.2$ WT (n=11), R333W (n=12), A343D (n=12), M518V (n=8), K526N (n=14), or R532W (n=18). **(E)** Immunoblotting with anti-Kv7.2 N-terminal antibodies on the lysate from CHO hm1 cells expressing Kv7.2 WT (n=4), R333W (n=12), A343D (n=4), M518V (n=4), K526N (n=4), or R532W (n=4).

GAPDH served as a loading control. Data shown represent the Ave ± SEM (*p<0.05, **p<0.01, ***p<0.005).

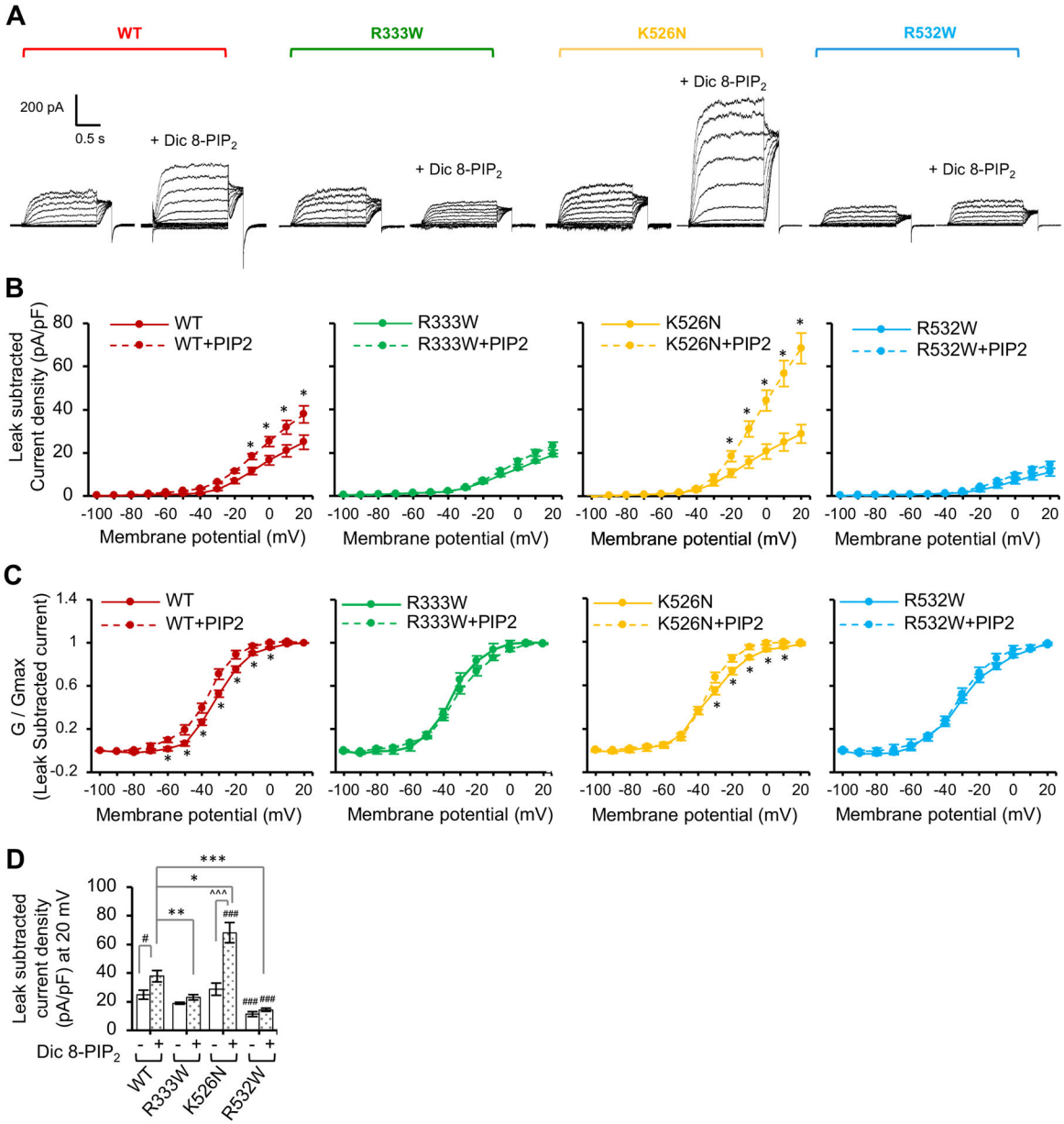

Figure 5. PIP_2 stimulation of $K_V7.2$ current is decreased by R333W and R532W mutations and increased by K526N mutation.

Whole cell patch clamp recording of $K_V7.2$ currents from CHO hm1 cells with or without diC8-PIP_2 (100 μM) in the patch pipette solution using the same voltage clamp protocol as described in Figure 4. The raw current traces and data are shown in Supplemental Fig. S4. **(A)** Representative leak-subtracted current traces. **(B-C)** Average peak current densities (B) and normalized conductance (G / Gmax) (C) were quantified using leak subtracted currents at all voltage steps. **(D)** Average leak subtracted peak current densities at + 20 mV in the absence or presence of diC8-PIP_2. The number of GFP-cotransfected cells that were analyzed without diC8-PIP_2: $K_V7.2$ WT (n=11), R333W (n=12), K526N (n=14), or R532W (n=18). The number of GFP-cotransfected cells that were analyzed with diC8-PIP_2: $K_V7.2$ WT (n=8), R333W (n=13), K526N (n=14), or R532W (n=11). Data shown represent the Ave

± SEM (#p<0.05, ###p<0.005 compared to WT without diC8-PIP_2, *p<0.05, **p<0.01, ***p<0.005 compared to WT with diC8-PIP_2, and ^^^p<0.005 compared to K526N without diC8-PIP_2)

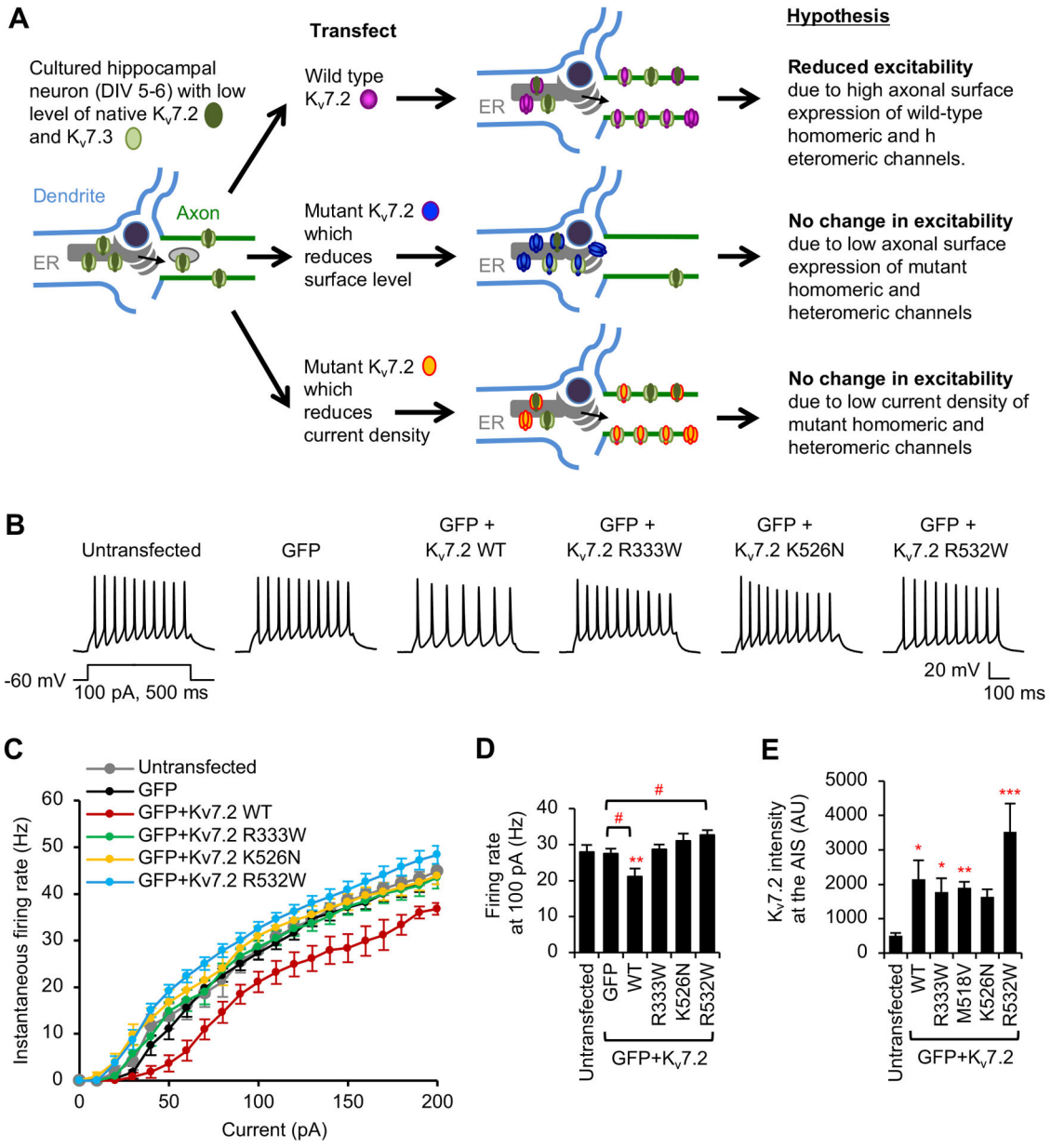

Figure 6. Hippocampal neuronal excitability is reduced upon expression of wild-type $K_V7.2$ but not $K_V7.2$ containing R333W, K526N, and R532W mutations.

Whole-cell current clamp recording in hippocampal neurons (DIV 6–8) transfected with GFP and $K_V7.2$ WT or $K_V7.2$ containing epileptic encephalopathy mutations. Spike trains were evoked by delivering constant somatic current pulses for 500 ms duration at a resting potential of –60 mV. **(A)** Hypothesis by which exogenously expressed $K_V7.2$ WT would decrease neuronal excitability by increasing expression of functional homomeric and heteromeric channels formed with endogenous $K_V7.2$ and $K_V7.3$ subunits. **(B)** Representative traces of action potentials induced by 100 pA injection. **(C)** Average instantaneous AP firing rates (Hz) induced by 0–200 pA injection. **(D)** Average firing rates at 100 pA from untransfected neurons (None: n = 9), or neurons transfected with GFP (n = 10), GFP and WT (n = 11), R333W (n = 9), K526N (n = 9), or R532W (n = 9). Data shown

represent the Ave ± SEM (** $p < 0.01$ compared to untransfected, $^{\#}p < 0.05$ compared to GFP).

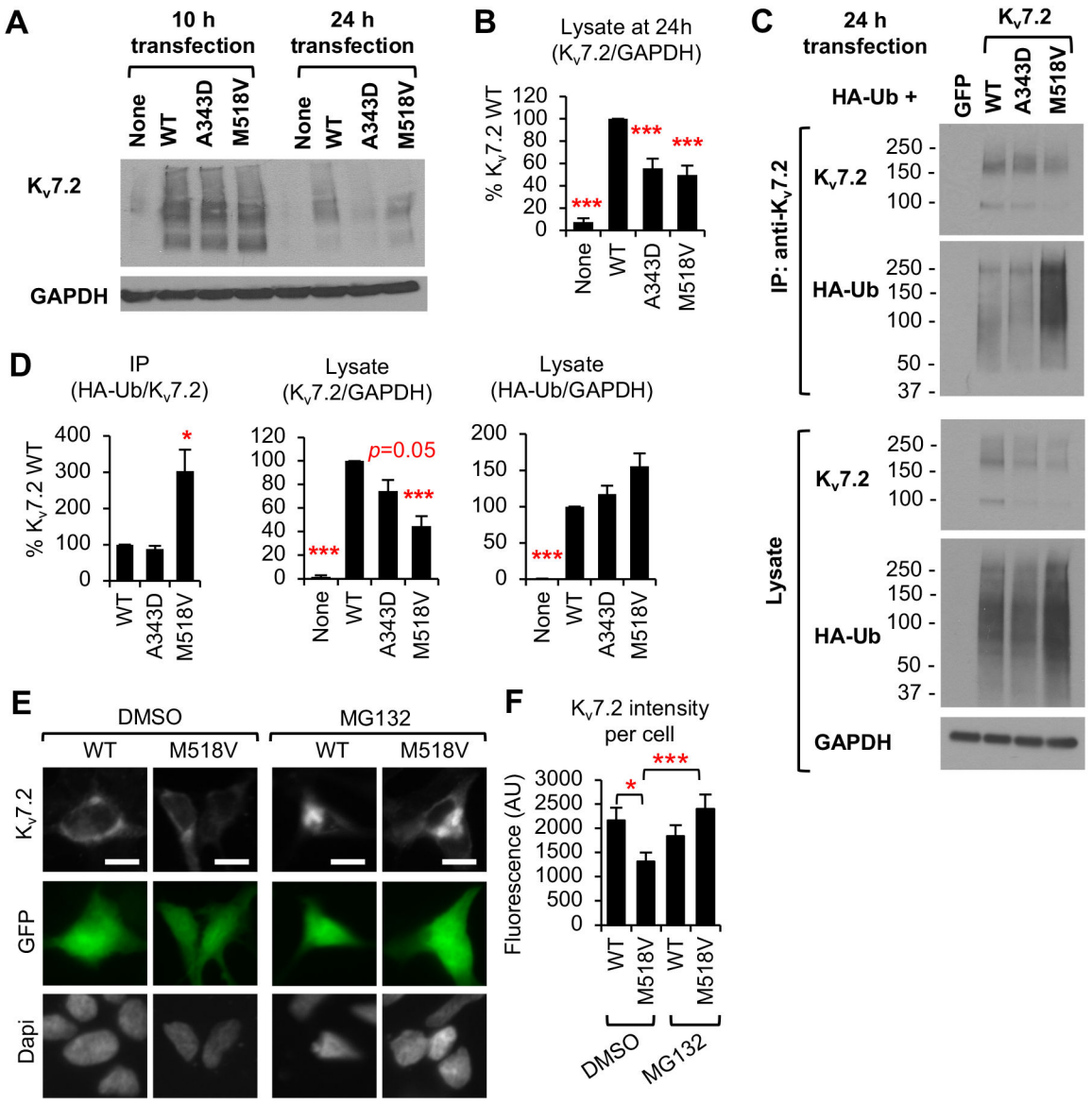

Figure 7. M518V mutation causes ubiquitination and proteasome-dependent degradation of $K_V7.2$.

(A-B) Immunoblot analyses of $K_v7.2$ WT, or mutant $K_v7.2$ (A343D and M518V) in HEK293T cells at 10 h and 24 h post transfection. Representative immunoblots (A). Quantification at 24 h post transfection for n=4 independent experiments. (B). **(C-D)** Immunoprecipitation of $K_v7.2$ WT or mutant $K_v7.2$ (A343D and M518V) from HEK293T cells cotransfected with HA-ubiquitin. Representative immunoblots (C). Quantification of coIP and lysate (D) are shown for n=4 independent experiments. **(E-F)** Immunocytochemistry of HEK293T cells showing total $K_v7.2$ WT or $K_v7.2$-M518V proteins after 24 h treatment with vehicle control DMSO (1% v/v) or MG132 (1 μM). Dapi staining shows nuclei. **(E)** Representative images with scale bars: 10 μm. **(F)** Background subtracted mean intensity of total $K_v7.2$ fluorescence per transfected cell for DMSO+WT

(n=20), DMSO+M518V (n=21), MG132+WT (n=22), MG132+M518V (n=22). Data shown represent the Ave ± SEM (*p<0.05, **p<0.01, ***p<0.005).

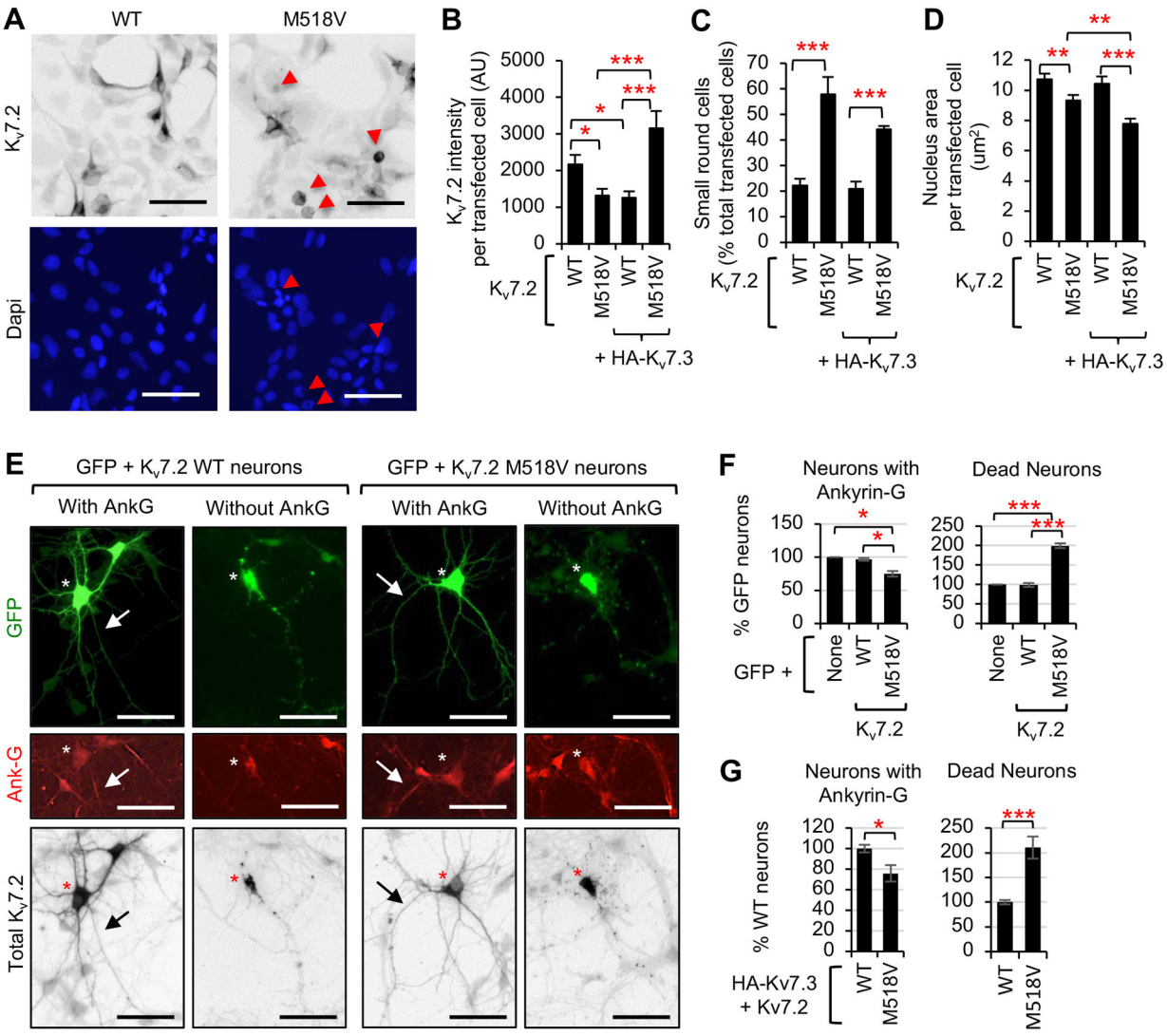

Figure 8. Expression of $K_v7.2$ causes cell death in transfected HEK293T cells and hippocampal neurons.

(A) Immunocytochemistry of $K_v7.2$ in HEK293T cells at 24 h post transfection. Dapi staining shows nuclei. **(B-D)** Immunocytochemistry of GFP-positive HEK293T cells cotransfected with $K_v7.2$ WT or M518V alone, or together with HA-$K_v7.3$. Representative images are shown in Supplemental Fig. S5. **(B)** Background subtracted mean intensity of total $K_v7.2$ fluorescence per transfected cell. **(C)** Quantification of small round transfected cells with average area of 9.9 ± 0.2 μm^2 as % transfected cells per image. Total number of transfected cells analyzed in n=10–18 images: $K_v7.2$-WT (n=507), $K_v7.2$-M518V (n=389), HA-$K_v7.3$+$K_v7.2$-WT (n=186), and HA-$K_v7.3$+$K_v7.2$-M518V (n=731). The average area of untransfected cells was of 14.5 ± 0.6 μm^2. **(D)** Average nucleus area per transfected cell. Total number of transfected cells analyzed: $K_v7.2$-WT (n=40), $K_v7.2$-M518V (n=38), HA-$K_v7.3$+$K_v7.2$-WT (n=40), and HA-$K_v7.3$+$K_v7.2$-M518V (n=39). Data shown represent the Ave ± SEM (*p<0.05, **p<0.01, ***p<0.005). **(E, F)** Immunocytochemistry of hippocampal neurons transfected with GFP and $K_v7.2$ WT or $K_v7.2$-M518V. **(E)**

Representative images. Ankyrin-G immunostaining marked the AIS (arrows). Cotransfected GFP allowed visualization of all neurites. Scale bars: 50 μm. **(F)** Quantification of the number of healthy transfected neurons containing prominent ankyrin-G immunostaining (Neurons with Ankyrin-G) and transfected neurons that had beaded or broken dendrites or axons, or damaged soma (Dead neurons) as % transfected cells. Total number of transfected neurons analyzed in n=4 independent experiments: GFP (n=300), GFP+K_v7.2-WT (n=252), GFP+K_v7.2-M518V (n=350). **(G)** Immunocytochemistry of hippocampal neurons transfected with HA-K_v7.3 and K_v7.2 WT or M518V was performed and quantified for live neurons with ankyrin-G and dead neurons as % transfected cells. Total number of transfected neurons analyzed in n=3 independent experiments: HA-K_v7.3+K_v7.2-WT (n=145), HA-K_v7.3+K_v7.2-M518V (n=183). Data shown represent the Ave ± SEM (*$p<0.05$, ***$p<0.005$).

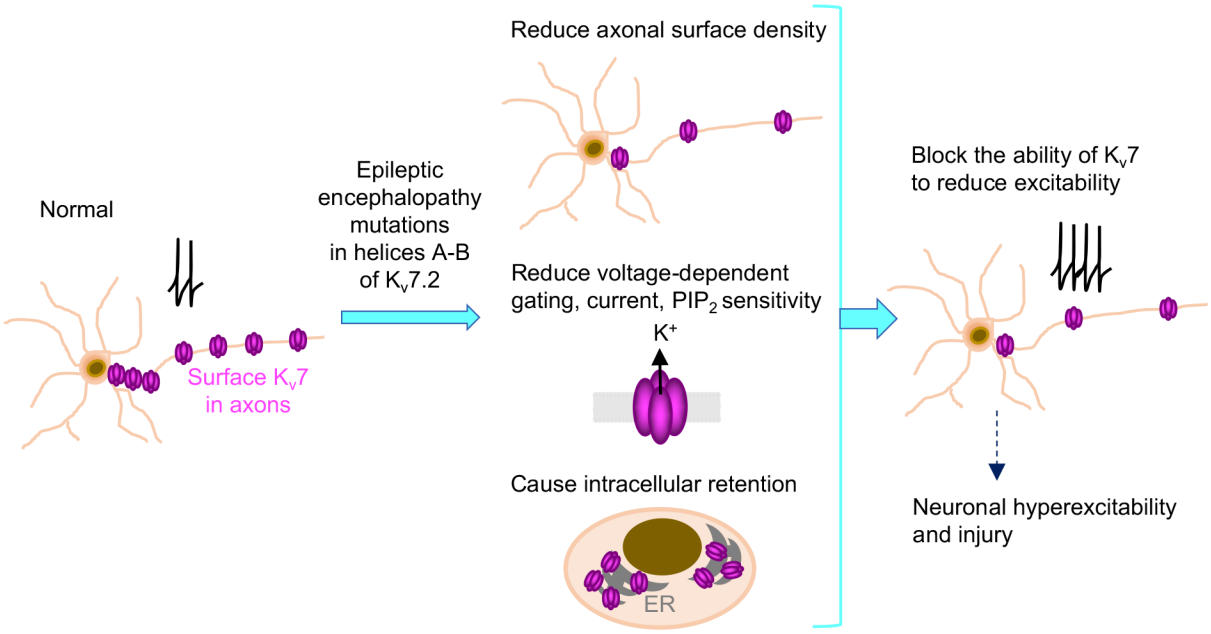

Figure 9. A working model for pathogenic mechanisms of epileptic encephalopathy mutations in helices A and B of K_v7.2.

Epileptic encephalopathy mutations (R333W, K526N, and R532W) localized peripheral to CaM contact sites in helices A and B reduced axonal surface expression of K_v7 channels, altered their sensitivity to PIP_2, and disrupted their ability to inhibit excitability in hippocampal neurons. In contrast, M518V mutation at the CaM contact site in helix B severely decreased CaM binding, axonal surface expression, and voltage-dependent activation. Intracellular accumulation of K_v7.2-M518V also caused cell death. We propose that a combination of these multiple yet diverse defects in K_v7 channels could exert more severe impacts on neuronal excitability and health, and thus serve as pathogenic mechanisms underlying *Kcnq2* epileptic encephalopathy.

Table 1.

Passive properties of CHO hm1 cells transfected with GFP and $K_v7.2$ containing epileptic encephalopathy mutations.

	Without diC8-PIP$_2$				*With diC8-PIP$_2$*			
Transfection	***n***	***V*$_m$ (mV)**	***C*$_m$ (pF)**	***E*$_{rev}$ (mV)**	***n***	***V*$_m$ (mV)**	***C*$_m$ (pF)**	***E*$_{rev}$ (mV)**
GFP	9	−10.2 ± 0.7*	11.9 ± 2.1	−25.6 ± 1.6*	ND	ND	ND	ND
GFP + $K_v7.2$ WT	11	37.0 ± 1.1	14.4 ± 1.5	−37.0 ± 1.1	8	−36.6 ± 1.5	17.2 ± 1.1	−44.6 ± 1.7‡
GFP + $K_v7.2$ A343D	12	−9.2 ± 0.5*	13.2 ± 0.7	−25.5 ± 2.3*	ND	ND	ND	ND
GFP + $K_v7.2$ R333W	12	−39.3 ± 1.4	14.7 ± 1.3	−40.5 ± 1.9	13	−37.1 ± 1.4	17.1 ± 1.4	−44.7 ± 2.1‡
GFP + $K_v7.2$ M518V	8	−28.5 ± 1.6*	22.0 ± 5.9	−29.9 ± 3.7*	ND	ND	ND	ND
GFP + $K_v7.2$ K526N	14	−37.1 ± 1.4	17.7 ± 3.0	−43.1 ± 0.8*	14	−42.7 ± 1.8†‡	17.8 ± 1.3	−53.1 ± 2.2†‡
GFP + $K_v7.2$ R532W	18	−35.3 ± 1.3	17.8 ± 1.9	−37.0 ± 1.9	11	−36.3 ± 1.2	17.6 ± 1.2	−45.0 ± 1.2‡

n, number; V_m, resting membrane potential; C_m, whole cell membrane capacitance; E_{rev}, reversal potential. Ave ± SEM (*p<0.05 compared to $K_V7.2$ wild-type (WT); †p<0.05 for $K_V7.2$ WT + diC8-PIP_2. vs mutants + diC8-PIP_2; ‡p<0.05 for $K_V7.2$ WT vs mutants + diC8-PIP_2). ND, not determined. Each value represents the Ave ± SEM.

Table 2.

Biophysical properties of wild-type and mutant $K_v7.2$ channels in GFP-cotransfected CHO hm1 cells in the presence or absence of diC8-PIP_2.

Transfection	*n*	*Leak substracted peak current* (pA)	$V_{1/2}$ (mV)	*k* (mV/efold)	$I_{instant}$ / $I_{steady\text{-}state}$	*Tau activation at +20 mV (ms)*
GFP + $K_v7.2$ WT	11	321.4 ± 38.5	−8.0 ± 0.6	10.6 ± 0.5	0.14 ± 0.02	79.4 ± 4.8
GFP + $K_v7.2$ A343D	12	15.6 ± 1.8*	−45.2 ± 3.3*	11.3 ± 2.5	1.00 ± 0.04*	4.9 ± 0.6*
GFP + $K_v7.2$ R333W	12	241.7 ± 35.5	−8.2 ± 1.1	12.5 ± 1.1	0.26 ± 0.02*	90.3 ± 6.3
GFP + $K_v7.2$ M518V	8	29.5 ± 8.2*	−32.9 ± 3.6*	10.2 ±1.5	0.89 ± 0.09*	5.2 ± 0.9*
GFP + $K_v7.2$ K526N	14	430.0 ± 72.2	−7.9 ± 0.9	14.5 ± 0.7*	0.11 ± 0.02	86.3 ± 2.9
GFP + $K_v7.2$ R532W	18	184.8 ± 30.5	−7.2 ± 1.4	12.2 ± 1.1	0.31 ± 0.04*	112.8 ± 7.2*
GFP + $K_v7.2$ WT + diC8-PIP2	8	638.4 ± 66.2‡	−6.4 ± 1.2	15.0 ± 0.5†	0.12 ± 0.02	79.7 ± 5.4
GFP + $K_v7.2$ R333W + diC8-PIP2	13	404.8 ± 54.6†	−7.9 ± 1.2	15.2 ± 1.0‡	0.19 ± 0.02‡	86.2 ± 2.9
GFP + $K_v7.2$ K526N + diC8-PIP2	14	1276.5 ± 140.8†‡	−5.3 ± 1.3‡	14.2 ± 0.8‡	0.07 ± 0.01‡	58.3 ± 2.4†‡
GFP + $K_v7.2$ R532W + diC8-PIP2	11	258.0 ± 31.3†	−5.6 ± 0.9	17.2 ± 2.6‡	0.21 ± 0.05†‡	100.3 ± 5.1‡

n, number; *Leak subtracted peak current* measured at +20 mV; $V_{1/2}$, half-activation potential calculated using leak subtracted currents; *k*, the slope factor calculated using leak subtracted currents; $I_{instant}$, leak subtracted current measured at the beginning of the depolarization step; $I_{steady\text{-}state}$, leak subtracted current measured at the end of the 0 mV depolarization; τ, activation time constant measured at + 20 mV using leak subtracted currents. Ave ± SEM (*p<0.05 for comparing $K_V7.2$ wild-type (WT) vs. mutants; †p<0.05 for comparing $K_V7.2$ WT + diC8-PIP_2. vs mutants + diC8-PIP_2; ‡p<0.05 comparing for $K_V7.2$ wild-type (WT) vs mutants + diC8-PIP_2). Each value represents the Ave ± SEM.

Table 3.

Passive properties of hippocampal pyramidal neurons transfected with GFP and $K_v7.2$ containing epileptic encephalopathy mutations.

Transfection	*n*	V_m (mV)	C_m (pF)	R_{in} (MΩ)
Untransfected	9	−54.5 ± 1.6	46.7 ± 2.5	873 ± 85
GFP	10	−52.4 ± 1.9	46.3 ± 3.3	819 ± 42
GFP + $K_v7.2$ WT	11	−52.4 ± 1.8	45.3 ± 1.3	858 ± 65
GFP + $K_v7.2$ R333W	9	−53.6 ± 2.0	46.3 ± 1.7	844 ± 44
GFP + $K_v7.2$ K526N	9	−52.8 ± 0.9	47.6 ± 2.7	881 ± 98
GFP + $K_v7.2$ R532W	9	−52.5 ± 2.1	48.6 ± 3.5	880 ± 34

n, number; V_m, resting membrane potential; C_m, whole cell membrane capacitance; R_{in}, input resistance. Each value represents the Ave ± SEM.

Table 4.

Action potential properties of hippocampal pyramidal neurons transfected GFP and $K_v7.2$ containing epileptic encephalopathy mutations.

Transfection	V_T (mV)	AP height (mV)	AP rise time (ms)	AP decay time (ms)	AP HW (ms)	fAHP (mV)
Untransfected	−31.0 ± 1.4	47.7 ± 3.9	1.04 ± 0.08	2.18 ± 0.27	2.50 ± 0.15	−17.4 ± 1.9
GFP	−33.9 ± 1.1	53.3 ± 3.8	1.10 ± 0.08	2.62 ± 0.27	2.78 ± 0.20	−15.2 ± 1.3
GFP + $K_v7.2$ WT	−32.8 ± 1.0	56.5 ± 2.5	1.14 ± 0.11	3.91 ± 0.40 $^{*,\#}$	3.54 ± 0.26 $^{*,\#}$	−12.1 ± 2.1 *
GFP + $K_v7.2$ R333W	−32.8 ± 1.1	48.7 ± 2.2	1.05 ± 0.06	2.92 ± 0.43 $^{\$}$	3.03 ± 0.23	−12.8 ± 1.7
GFP + $K_v7.2$ K526N	−35.0 ± 0.8 *	54.3 ± 3.1	1.20 ± 0.08	2.93 ± 0.22 $^{\$}$	2.98 ± 0.19	−10.5 ± 1.5 *
GFP + $K_v7.2$ R532W	−34.2 ± 1.0	53.5 ± 3.3	1.21 ± 0.10	2.57 ± 0.23 $^{\$}$	2.83 ± 0.15 $^{\$}$	−12.8 ± 0.8

V_T, voltage threshold for action potential; AP, Action potential; rise, 10–90% rise time of AP; decay, 10–90% decay time of AP; HW, half-width; fAHP, fast after-hyperpolarization. AP properties were measured from the first action potential evoked by a current step to 100 pA at a holding potential of −60mV. Each value represents the Ave ± SEM.

* $p<0.05$ compared to untransfected;

$^{\#}$ $p<0.05$ compared to GFP;

$^{\$}$ $p<0.05$ compared to WT.